blood®
Regular Article

LYMPHOID NEOPLASIA

A comprehensive genetic study of classic Hodgkin lymphoma using circulating tumor DNA

Maria Cristina Pirosa,[1-3,*] Alessio Bruscaggin,[1,*] Lodovico Terzi di Bergamo,[1,4,5,*] Matin Salehi,[1,3,4,*] Federico Jauk,[1,3] Gabriela Forestieri,[1] Simone Bocchetta,[1] Deborah Piffaretti,[1] Riccardo Moia,[6] Vanessa Cristaldi,[7] Martina di Trani,[7] Georgia Alice Galimberti,[1] Katia Pini,[1] Valeria Spina,[1] Claudia Giordano,[8] Adalgisa Condoluci,[1-3] Ilaria Romano,[1-3] Salvatore Annunziata,[9] Fabrizio Bergesio,[10] Renzo Boldorini,[11] Eugenio Borsatti,[12] Pietro Bulian,[13] Eleonora Calabretta,[7] Stephane Chauvie,[10] Francesco Corrado,[7] Stefania Crisci,[14] Marco Cuzzocrea,[15] Rosaria De Filippi,[8] Bernhard Gerber,[2] Michał Kurlapski,[16] Luigi Maria Larocca,[17] Elisabetta Merlo,[18] Andrea Rinaldi,[19] Marcello Rodari,[20] Grzegorz Romanowicz,[21] Gian Mauro Sacchetti,[22] Anastasios Stathis,[2] Georg Stüssi,[2,3] Ilaria Zangrilli,[23] Antonello Pinto,[14] Luca Mazzucchelli,[18] Valter Gattei,[13] Jan Maciej Zaucha,[16] Armando Santoro,[24] Stefan Hohaus,[23] Franco Cavalli,[25] Alexandar Tzankov,[26] Carmelo Carlo-Stella,[7,24] Gianluca Gaidano,[6,†] Luca Ceriani,[3,15,†] Emanuele Zucca,[2,3,†] and Davide Rossi[1-3,†]

[1]Laboratory of Experimental Hematology, Institute of Oncology Research, Bellinzona, Switzerland; [2]Clinic of Hematology, Oncology Institute of Southern Switzerland, Ente Ospedaliero Cantonale, Bellinzona, Switzerland; [3]Faculty of Biomedical Science, Università della Svizzera Italiana, Lugano, Switzerland; [4]Bioinformatics Core Unit, Swiss Institute of Bioinformatics, Bellinzona, Switzerland; [5]Department of Health Science and Technology, Swiss Federal Institute of Technology, ETH Zürich, Zürich, Switzerland; [6]Division of Hematology, Department of Translational Medicine, University of Eastern Piedmont, Novara, Italy; [7]Department of Biomedical Sciences, Humanitas University, Milan, Italy; [8]Department of Clinical Medicine and Surgery, Federico II University Medical School, Naples, Italy; [9]UOC Medicina Nucleare, GSTeP Radiopharmacy TracerGLab, Fondazione Policlinico Universitario A. Gemelli IRCCS, Rome, Italy; [10]Department of Medical Physics, Santa Croce e Carle Hospital, Cuneo, Italy; [11]Pathology Department, Ospedale Maggiore della Carità, University of Eastern Piedmont, Novara, Italy; [12]Nuclear Medicine and [13]Clinical and Experimental Onco Hematology Unit, Centro di Riferimento Oncologico, Aviano, Italy; [14]Hematology-Oncology and Stem Cell Transplantation Unit, Istituto Nazionale Tumori-IRCCS-Fondazione "G. Pascale," Naples, Italy; [15]Clinic of Nuclear Medicine and Molecular Imaging, Imaging Institute of Southern Switzerland, Bellinzona, Switzerland; [16]Department of Hematology and Bone Marrow Transplantation, Medical University of Gdańsk, Gdańsk, Poland; [17]Division of Pathology, Fondazione Policlinico Universitario Agostino Gemelli, Catholic University of the Sacred Heart, Rome, Italy; [18]Division of Pathology, Ente Ospedaliero Cantonale, Locarno, Switzerland; [19]Genomics Facility, Institute of Oncology Research, Bellinzona, Switzerland; [20]Unit of Nuclear Medicine, Humanitas Research Hospital, Milan, Italy; [21]Department of Nuclear Medicine, Medical University of Gdańsk, Gdańsk, Poland; [22]Nuclear Medicine, Ospedale Maggiore della Carità, Novara, Italy; [23]Department of Diagnostic Imaging, Oncological Radiotherapy and Hematology, Fondazione Policlinico Universitario Agostino Gemelli, Rome, Italy; [24]Department of Oncology and Hematology, Humanitas Research Hospital, Milan, Italy; [25]Fondazione per l'Istituto Oncologico di Ricerca, Bellinzona, Switzerland; and [26]Department of Histopathology and Autopsy, Institute of Medical Genetics and Pathology, University Hospital Basel, Basel, Switzerland

KEY POINTS

- **The genetic subtypes of cHL are driven more by mechanisms of genetic instability than by clustering of mutations into functional groups.**
- **Noncoding mutations of BCL6, whole genome duplication, and neoantigens are involved in shaping the pathophysiology and outcome of cHL.**

This study analyzed the genetics of classic Hodgkin lymphoma (cHL) by using circulating tumor DNA (ctDNA). Two genetic subtypes were identified, differing in genetic instability mechanisms: one subtype (64% of cases) showed a higher mutation load and a higher fraction of mutations associated with activation-induced cytidine deaminase and microsatellite instability signatures, whereas the other subtype (36% of cases) exhibited chromosomal instability with more somatic copy number alterations. Whole-genome duplication was more common in cHL compared with other B-cell tumors and emerged as a prognostic biomarker for patients undergoing Adriamycin (doxorubicin)-bleomycin-vinblastine-dacarbazine–based therapy. Noncoding regulatory mutations, similar to those in diffuse large B-cell lymphoma, were highly prevalent in 86% of cHL. A recurrent somatic expression quantitative trait locus (seQTL) involving the *BCL6* gene was found in 30% of cases. The seQTL of *BCL6* aligned with accessible chromatin and increased H3K27 acetylation in cHL, disrupted PRDM1 binding, and co-occurred with BCL6 expression in cHL cells. Weak to strong expression of BCL6 was observed in 68% of cases, and BCL6 expression associated with gene repression similarly in cHL and germinal center B cells. After BCL6 degradation, the core set of genes directly bound and regulated by BCL6 was derepressed in cHL, and proliferation was impaired. The number and clonality of neoantigens was associated with tumor microenvironment type and response to checkpoint blockade. Finally, ctDNA analysis was suggested as a tool to distinguish ambiguous positron emission tomography/computed tomography–positive lesions after treatment.

Introduction

Genetic research on classic Hodgkin lymphoma (cHL) has been limited by the scarcity of Hodgkin/Reed-Sternberg (HRS) cells in tissue, requiring enrichment for analysis. This has hindered efforts to identify distinct genetic subtypes, to connect genetics with aspects of the pathophysiology of the disease, such as microenvironment composition, cytokine deregulation, and Epstein-Barr virus (EBV) infection, and to explore the clinical significance of genomic abnormalities.[1-7] Plasma from patients with cHL shows a higher concentration of neoplastic DNA than the bulk tumor, making circulating tumor DNA (ctDNA) ideal for noninvasive molecular profiling.[5,8-13]

In diffuse large B-cell lymphoma (DLBCL), noncoding regions, including superenhancers (SEs), often undergo activation-induced cytidine deaminase (AID)–associated somatic hypermutation (SHM), leading to deregulation of proto-oncogenes involved in germinal center (GC) biology and malignancy.[14] Although cHL also arises from GC B cells, AID-associated SHM in noncoding regions has not yet been studied in cHL.

Given cHL high curability, a focus of clinical research is on personalizing treatment by deescalating therapy to reduce long-term complications.[15,16] Positron emission tomography/computed tomography (PET/CT) scans help guide treatment adjustments,[17] but ≈25% of results are false positives,[18] potentially leading to unnecessary interventions.

We used ctDNA analytics to detail cHL genetic landscape, its connection to disease biology and outcome, and to evaluate ctDNA-based molecular response vs PET/CT restaging.

Materials and methods

Patient characteristics

The study included 307 cases from 2 multicenter studies evaluating ctDNA in cHL (297 assessable: dropout reasons are reported in CONSORT of supplemental Figure 1, available on the *Blood* website). IOSI-EMA003 enrolled newly presented patients with cHL treated according to local policies and those with relapsed/refractory disease treated with checkpoint inhibitors. FIL-RougeBIO, part of the FIL-Rouge clinical trial, recruited young advanced-stage patients with cHL receiving Adriamycin (doxorubicin)-bleomycin-vinblastine-dacarbazine (ABVD)–based first-line therapy (Table 1; supplemental Figure 2). PET/CT scans were centrally reviewed for pretreatment metabolic tumor volume (MTV)[19] and response per Deauville criteria.[20] Blood samples were collected in cell-free DNA-preserving tubes during PET/CT staging and response assessments. Additional information on patient cohorts and PET/CT review process are in the supplemental Methods.

ctDNA genotyping

A selector spanning 344 kb was optimized, comprising 33 AID-associated SHM-hit noncoding regions[1,21-23] contained within SE of GC B cells,[14] and various coding regions of 155 recurrently mutated genes in mature B-cell tumors (supplemental Table 1). Somatic mutation enrichment of our selector was compared with that of meta-data from whole-genome sequencing and whole-exome sequencing studies in cHL.[1,2,4] Despite covering only 0.01% of the human genome, our selector achieved an 11- and 210-fold increase in mutation detection per sample and per sequenced base pair for coding and noncoding mutations, respectively. Expanding the genomic area beyond our selector was expected to yield only a slight increase in detecting recurrent mutations (supplemental Figure 3A-B).

The genomic region of the selector was sequenced in plasma cfDNA and paired germ line DNA using a Cancer Personalized Profiling by Deep Sequencing (CAPP-seq) library preparation protocol and the Illumina platform[24] (median unique coverage depth: ~4000×). An error-suppressing bioinformatics was used to detect somatic mutations,[24,25] whereas genome-wide somatic copy number abnormalities (SCNA) were inferred from off-target reads.[26-30] When applied to posttreatment cfDNA samples from 119 patients cured of lymphoma (ie, "blank" samples), the limit of quantification for the CAPP-seq assay for mutation detection was determined to be 0.17%. This threshold represents the level of analytical background noise above which the assay generates a signal distinguishable from the "blank" samples (supplemental Figure 3E). In dilution experiments mixing cfDNA from patients with cHL with that from healthy donors, our assay demonstrated an analytical sensitivity of 0.1% for residual ctDNA identification (supplemental Figure 3F). The analytical sensitivity for SCNA was 3%, as in the dilution experiment, and 3% was the cancer cell fraction at which we were able to call SCNA that existed in the undiluted sample.

The assay diagnostic performance was assessed by comparing sequencing results from cfDNA with those from genomic DNA of flow-sorted HRS cells (supplemental Figures 3G-H, and 4), achieving a 93% sensitivity in detecting confirmed somatic mutations from tumor cells. The diagnostic accuracy for SCNA detection in ctDNA was confirmed by comparison with a low-pass whole-genome sequencing experiment (supplemental Figure 3C-D).[31] The diagnostic accuracy in detecting whole-genome duplication (WGD) was confirmed by comparing its results with the ploidy status determined through conventional cytogenetics in lymphoma cell lines (supplemental Figure 3I).

Other methods

The supplementary methods provide detailed information on the methods used for pathology review, tissue microarray, chromatin immunoprecipitation sequencing, assay for transposase-accessible chromatin with sequencing, RNA sequencing, EBV detection, plasma cytokine measurement, HLA typing, and in vitro assays.

Statistical analysis

Progression-free survival (PFS) was defined according to the International Working Group response criteria.[32] Interim and end of treatment PET/CT results were assessed according to the Lugano 2014 criteria.[20] Summary statistics for continuous variables included median and quartiles or mean and standard deviation (SD), depending on the normality of the data distribution. Categorical data were presented as percentages and 95% confidence interval (CI), and compared by Fisher exact test. Survival analysis was performed by the Kaplan-Meier method, whereas comparison of the strata was performed

Table 1. Clinical characteristics of patients with cHL

Characteristic	Treatment naïve IOSI-EMA003 (n = 215)		Treatment naïve FIL-RougeBIO (n = 45)		Relapsed/refractory IOSI-EMA003 (n = 37)	
Age, median/range, y	39	16-84	39	18-59	30	16-80
Male	110	51%	27	60%	21	57%
ECOG PS >1	13	6%	1	4%	2	5%
Histology						
Mixed cellularity	24	11%	5	11%	2	5%
Nodular sclerosis	161	75%	35	78%	33	90%
Other	30	14%	5	11%	2	5%
Ann Arbor stage III-IV	112	52%	37	82%	26	70%
GHSG stage						
Early favorable	19	9%	0	0%	—	—
Early unfavorable	67	31%	0	0%	—	—
Advanced	129	60%	45	100%	—	—
B symptoms	104	48%	25	56%	15	40%
Large mediastinal mass	52	24%	17	38%	—	—
Extranodal involvement	80	37%	—	—	—	—
≥3 Nodal areas	174	81%	—	—	—	—
Elevated ESR	141 (n = 209)	67%	30 (n = 38)	79%	—	—
IPS >2	74	34%	19	42%	—	—
EBV positivity	29 (n = 169)	17%	—	—	—	—
MTV, median, mL	115 (n = 196)	0-1742	—	—	—	—
Treatment						
ABVD	163	76%	45	100%	0	0%
eBEACOPP	17	8%	0	0%	0	0%
ABVD-like	35	16%	0	0%	0	0%
Nivolumab	0	0%	0	0%	28	76%
Pembrolizumab	0	0%	0	0%	7	19%
Other CPI	0	0%	0	0%	2	5%
Unplanned RT	23	11%	6	13%	—	—
iPET pos	31 (n = 212)	15%	—	—	—	—
Follow-up, median/95% CI, mo	29	26-32	28	25-31	33	13-53

—, not available or not applicable; ABVD, Adriamycin-bleomycin-vinblastine-dacarbazine; CI, confidence interval; CPI, checkpoint inhibitor; eBEACOPP, escalated bleomycin-etoposide-adryamycin-cyclophosphamide-vincristine-procarbazine-prednsione; ECOG, Eastern Cooperative Oncology Group; ESR, erythrocyte sedimentation rate; GHSG, German Hodgkin Study Group; iPET, interim PET/CT; IPS, International Prognostic Score; MTV, metabolic tumor volume; RT, radiation therapy.

with the log-rank test. The association between PFS and exposure variables was estimated by Cox regression and reported as the hazard ratio (HR) and 95% CI. Significance was considered when *P* or multiplicity-adjusted *P* value was <.05. All statistical tests were 2 sided. The analysis was performed with IBM SPSS statistics 28.0 and R, version v3.6. Details on the bioinformatics are reported in the supplemental methods.

Results

Molecular profile of cHL

Somatic mutations were detected in 252 of 280 (90%) assessable cases (supplemental Figure 1A). Seventeen cases were not assessable for mutations because of enrichment of possible sequencing artefacts as confirmed by COSMIC single base substitutions (SBS) analysis. SCNA were detected in all 273

assessable cases. Twenty-four cases were not assessable for SCNA as they did not meet the quality control metrics. The median number per case of nonsynonymous mutations in known lymphoma genes (n = 6; range, 0-60) and of SCNA (n = 6; range, 0-47) was similar to that reported in previous genomic studies of cHL.[1-7] Fusions that recurred in at least 2 patients were observed in 32% of cases. None of the fusions was detected in >3 cases (supplemental Table 2). The absence of detectable ctDNA was associated only with low pretreatment tumor volume, as receiver operating characteristic analysis showed that an MTV >1 mL was sufficient for ctDNA detection.

The genes most frequently affected by nonsynonymous somatic mutations included *SOCS1*, *TNFAIP3*, *STAT6*, *B2M*, *GNA13*, and *ITPKB* (supplemental Figure 5A), consistent with the previous literature.[1-7] Focal SCNA included gains involving 2p16.1 (*REL*, *XPO1*), 3q27 (*BCL6*), 7q36.3 (*EZH2*), 9p24.2 (*JAK2*, *CD274*, and *PDCD1LG2*), 8q24.23 (*MYC*), 15q26.3 (*IGF1R*), as well as deletions involving 1p36.13 (*TNFRSF14*), 1p12 (*CD58*), 3q27.1 (*KLHL6*), 6q23.3 (*TNFAIP3*), 13q13.3 (*FOXO1*), 14q12 (*NFKBIA*), 15q25.3 (*B2M*), 16p13.3 (*CREBBP*), and 20q13.13 (*PTPN1*) (supplemental Figure 5B-E). Supplemental Figure 6 illustrates both the co-occurrence and the alternate presence of genetic abnormalities. Most cHL cases displayed a common genetic profile, characterized by frequent and co-occurring mutations in genes associated with just 2 pathways: cytokine signaling and the NF-κB (supplemental Figure 7).

EBV infection was assessed by in situ hybridization of the tumor biopsy and by quantitative polymerase chain reaction of EBV load in plasma.[33] EBV-positive cHL (17%) had a lower number of mutations and SCNA compared with EBV-negative cases (supplemental Figure 8A-E). By seeding EBV status and then cyclically adjusting cases between categories based on a genetic distinctiveness metric,[34] virtually all EBV-positive cHL cases were grouped together in a subset of cHL showing a high enrichment of *SOCS1* mutations but few *STAT6* mutations (supplemental Figure 9). Notably, 68% of cases of this subset, despite sharing a similar genetic profile with EBV-positive cases, lacked EBV (supplemental Figure 9), indicating that the genetic background of cHL is not primarily seeded by EBV infection.

Genetic subtypes of cHL are driven by mechanisms of genetic instability

The validity of our ctDNA assay for molecular clustering of lymphoma was evaluated by profiling ctDNA from 235 untreated DLBCL. Using nonnegative matrix factorization–based unsupervised clustering,[35] cases were assigned to the previously described subtypes C0 to C5 (C0 = 11%, C1 = 16%, C2 = 15%, C3 = 21%, C4 = 19%, and C5 = 19%) (supplemental Figures 10 and 11).[35]

In cHL, nonnegative matrix factorization–based unsupervised clustering identified 2 distinct subtypes (supplemental Figures 12 and 13). The hypermutated subtype (C1: 63% of cases) exhibited a higher mutation density, and was characterized by nonsynonymous mutations in coding genes targeted by AID hypermutation and by noncoding SHM in the *BCL6* intragenic SE (Figure 1A-B). C1 had a lower number of SCNA (Figure 1C). Consistent with the enrichment of *B2M*-disrupting mutations, C1 showed a higher number of predicted neoantigens (Figure 1D) and ratio of neoantigens over total number of mutations (supplemental Figure 14). The chromosomal instability subtype (C2: 35% of cases) was characterized by a higher SCNA burden and a lower mutation density (Figure 1A-B). Both subtypes shared hallmark lesions of cHL, such as *STAT6* mutations and gains at 2p/2p16.1 and 9p/9p24.2, and displayed similar baseline characteristics, including age, sex, histopathologic subtype, EBV infection, B symptoms, clinical stage, and ctDNA load (Figure 1A). The ctDNA load, along with the quantity and distribution of on- and off-target reads, showed no significant differences between C1 and C2 (supplemental Figure 15A-C).

A small subtype without detectable class-defining alterations (C0: 2%) was also identified (Figure 1A).

Compared with C2, the C1 subtype exhibited a higher proportion of cases with SBS84 mutations linked to AID (59% vs 43%; P = .021126) and SBS15 mutations associated with microsatellite instability (MSI) (14% vs 4%; P = .024883) (Figure 1E). Additionally, C1 showed greater densities of both SBS84 (mean mutation/Mpb: 30.7 ± 43.0 SD vs 16.3 ± 29.2 SD; P = .010013) and SBS15 (mean mutation/Mbp: 1.5 ± 5.8 SD vs 0.2 ± 1.0 SD; P = .031000) mutations compared with C2. Our selector included 30 MSI markers that we used to evaluate stability (mutations in >10% of MS) in ctDNA.[36] In line with the increased frequency of SBS15 mutations, we observed a significantly higher prevalence of MSI (10%-40% of markers affected) in C1 cases compared with C2 (Figure 1F).

These association-based observations suggest that the genetic subtypes of cHL might have been shaped by mechanisms of genetic instability, such as hypermutation and chromosomal instability, rather than by the clustering of mutations into specific functional categories or the influence of EBV infection.

Mutations of noncoding regulatory regions

Mutations in at least 1 noncoding regulatory region that is hotspot of AID-associated SHM[14] and that was encompassed by our selector were found in 83% of cHL cases, similar to DLBCL (88%) (supplemental Figure 16A), with many mutations showing AID signatures (SBS84, SBS85) (supplemental Figure 16B-C). Beyond *IG* loci (eg, *IGLL5*), the *BCL6* locus was the most frequently mutated in 56% of cHL (Figure 2A).

By scanning the sequenced genome in overlapping 20-bp intervals, 6 mutation hotspots with higher mutation frequency than background and recurring in >10% of cHL cases were identified. Four matched known coding hotspots of cHL in *STAT6*, *B2M*, *SOCS1*, and *XPO1* (Figure 2B; supplemental 16D) ,[1-7] confirming our method's accuracy. Additionally, a hotspot in *BCL6* (named hotspot 7) at chromosome 3:187462671-187462703 was found in 30.7% of cHL cases (Figure 2B-C).

BCL6 hotspot 7, located in the SE of *BCL6*-intron 1 in GC B cells,[14] aligned with accessible chromatin (supplemental Figure 17) and H3K27 acetylation in cHL cell lines (Figure 2D; supplemental Figure 18). Chromatin immunoprecipitation–sequencing analysis showed higher H3K27Ac levels in *BCL6* hotspot 7 mutant cHL cell lines, suggesting altered transcription factor binding (Figure 2E).

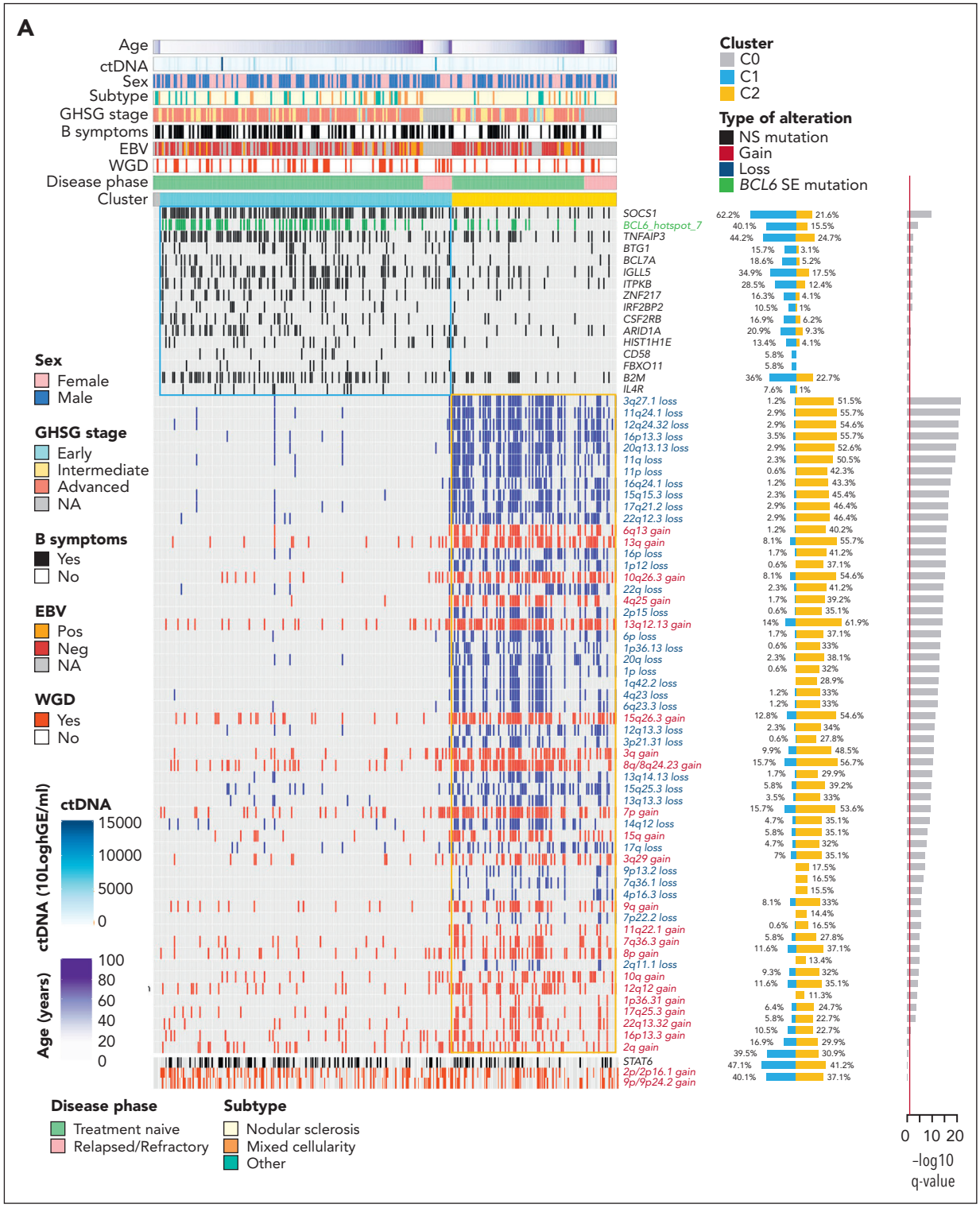

Figure 1. Consensus clustering identified 2 cHL subtypes distinguished by the underlying mechanisms of genetic instability. (A) Oncoprint showing the nonnegative matrix factorization consensus clustering performed using significant nonsynonymous mutations, SCNA and *BCL6* hotspot 7 mutations in 273 cHL samples (columns). Samples without driver alterations are represented as cluster C0 (gray). *P* value by Fisher test adjusted for multiplicity. The red bar marks the significance threshold. The header indicates pretreatment clinical features. (B) Box plot showing the median (the number within the box), quartiles, 95% percentiles, and extremes of the density of mutations within the genomic space of the selector that covers known hotspot of SHM in C1 and C2 subtypes. *P* values determined by Mann-Whitney test. (C) Box plot showing the median (the number within the box), quartiles, 95% percentiles, and extremes of the SCNA in C1 and C2 subtypes. *P* values determined by Mann-Whitney test. (D) Box plot showing the median (the number within the box), quartiles, 95% percentiles, and extremes of number of predicted neoantigens in C1 and C2 subtypes. *P* values determined by Mann-Whitney test. (E) Bar graphs of the mutation signatures of C1 top and C2 bottom. (F) Pie charts showing the prevalence of microsatellite stability (MSS) and MSI among C1 and C2 patients. *P* values determined by χ^2 test. NA, not available; Neg, negative; NS, nonsynonymous; Pos, positive.

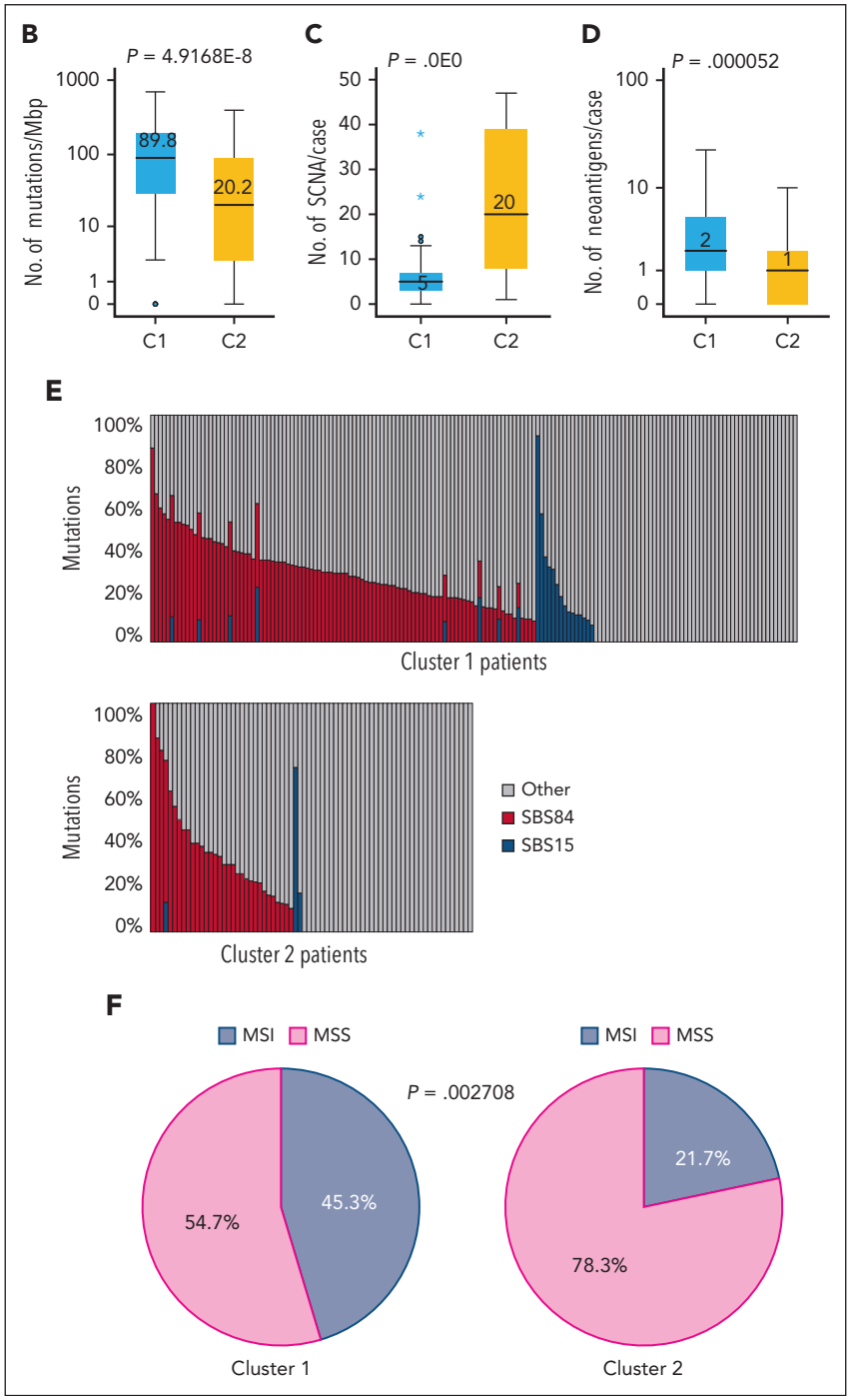

Figure 1 (continued)

The proportion of patients with cHL with *BCL6* hotspot 7 mutations was similar to that of DLBCL (supplemental Figure 16E), with chromosome 3:186472688 being the most affected nucleotide, and corresponded to a somatic expression quantitative trait locus (seQTL) of *BCL6*.[14] The wild-type sequence of *BCL6* hotspot 7 was predicted to be consensus for PRDM1 (Figure 3A), a transcriptional repressor of BCL6, and mutations therein were predicted to affect PRDM1 binding. *BCL6* hotspot 7 mutations co-occurred with BCL6 expression in cHL cell lines and HRS cells of primary biopsies, despite PRDM1 co-expression in some instances (Figure 3B-C). A total of 48 primary cHL biopsies were evaluated for *BCL6* hotspot 7 mutation along with BCL6 and PRDM1 immunohistochemistry expression. Of the 8 cases expressing PRDM1, 2 harbored *BCL6* hotspot 7 mutations, and both expressed BCL6.

The lengthy duplication time of the UHO1 cHL cell line, that carried *BCL6* hotspot 7 mutation and expressed both PRDM1 and BCL6, hampered genome editing to revert to wild-type *BCL6* hotspot 7 mutations. We therefore performed PRDM1 chromatin immunoprecipitation–quantitative polymerase chain reaction on the UOH1 cell line and on the AM-HLH cHL cell line

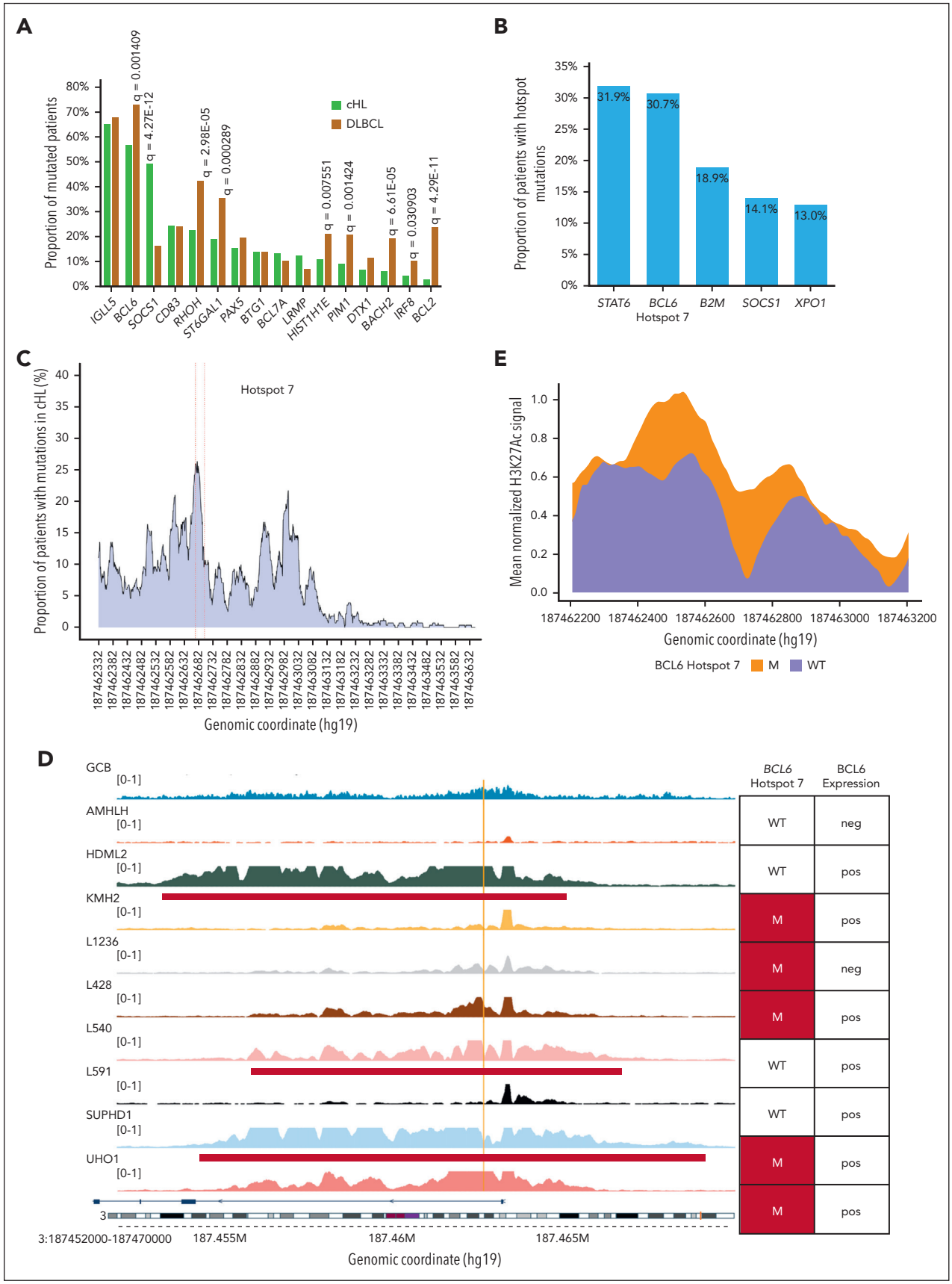

Figure 2. Mutations of noncoding regulatory regions. (A) Bar graph showing the prevalence of mutations of each individual hotspot of SHM that is covered by the selector in cHL and DLBCL. Q by χ^2 test adjusted for multiple comparisons. (B) Bar plot showing the prevalence of mutations within hotspot windows that recurs in >10% of cases of

that was wild type in *BCL6* hotspot 7 and expressed PRDM1 but not BCL6. Although PRDM1 binding was undetectable in the UHO1 mutated cells, it was significantly enriched in the AM-HLH wild-type cells (Figure 3D). These findings suggest *BCL6* hotspot 7 mutations hinder PRDM1 binding in cHL as in DLBCL.[14]

BCL6 is involved in a fraction of cHL

BCL6 protein expression ranging from weak to strong was detected in the nucleus of HRS cells of 68% of primary biopsies (supplemental Figure 19A-G). Gene expression profiles of microdissected HRS cells (n = 29) were compared with microdissected GC cells (n = 5) from Gene Expression Omnibus accession number GSE39133. The core set of genes that are directly bound and regulated by BCL6[37] exhibited similar expression levels in GC B cells and in BCL6 expressing cHL cell lines and in primary HRS cells[38] (supplemental Figure 19H-I). Furthermore, the core set of genes directly bound and regulated by BCL6 had a nearly identical chromatin accessibility pattern in GC B cells and in BCL6-expressing cHL cell lines (supplemental Figure 19L).

Degradation of the BCL6 protein was specifically promoted in cHL cell lines by using BI-3802.[39] BCL6 protein degradation was observed after 7 days of treatment with BI-3802 in 4 of the 7 cHL cell lines expressing BCL6 (Figure 3E). The core set of genes directly bound and regulated by BCL6[37] was derepressed in cHL cell lines that responded to BI-3802, but not in cHL cell lines where BI-3802 did not degrade BCL6 (Figure 3F). Compared with the BI-5372 control molecule, treatment with BI-3802 significantly decreased proliferation in all cell lines where BCL6 degradation was observed, as well as in the BCL6-dependent SUDHL4 DLBCL cell line (Figure 3G), with the peak effect expectedly occurring after 7 days of treatment.[40]

Overall, these findings indicate that BCL6 plays a role in transcriptional regulation of a fraction of cHL and represents a potential vulnerability in this subset.

Genetics in relation to outcome

Treatment-naïve cHL of the IOSI-EMA003 study formed the training cohort, mainly receiving ABVD across various stages and risk groups. Established cHL biomarkers were prognostic for PFS in the training cohort (Table 2). Univariate analysis revealed no correlation between gene mutations, focal- or arm-level SCNA, or *BCL6* hotspot 7 mutations with reduced PFS (supplemental Figure 20). Patients classified as C1 exhibited a nominally lower risk of progression than patients classified as C2 (HR, 0.513; 95% CI, 0.255-1.034; P = .061904).

The most notable characteristic of HRS cells is their binucleate or multinucleate polyploid appearance. A common feature of cancers that are enriched of polyploid giant cells is WGD, which has also been described in cHL,[1,4,41] and is associated with poor prognosis in cancer.[42] WGD was detected in ctDNA of 24% of patients with cHL, a frequency nominally higher than that seen in other mature B-cell malignancies (Figure 4A).

CCNE1 gain, along with *TP53* and *RB1* abnormalities are linked to WGD in solid tumors.[42,43] *CCNE1* gain was found in 13% of cHL cases, aligning with previous studies that reported recurrent gains on 19q13 in cHL.[44,45] *CCNE1* amplification was significantly associated with WGD, whereas *TP53* and *RB1* abnormalities were rare in cHL and did not correlate with WGD (Figure 4B-C).

From a clinical perspective, detection of WGD in ctDNA was significantly linked to a shorter PFS in the IOSI-EMA003 training cohort by univariate analysis (Figure 4D). In multivariate analysis, it emerged as an independent biomarker for prognosticating PFS after adjusting for clinical stage, international prognostic score, and MTV (Figure 4E). The association of WGD with inferior PFS was further confirmed in the FILRougeBIO validation cohort (Figure 4F).

WGD is more common in patients with C1 compared with C2 (27.9% vs 13.5%; P = .003019). The increased prevalence of WGD in C1 patients aligns with the established association between hypermutator phenotypes and the frequent co-occurrence of WGD in cancer.[46]

Collectively, this evidence supports WGD as a prognostic biomarker of untreated patients with cHL who received ABVD-based therapy.

Molecular aspects within the context of tumor microenvironment

The expression of 1402 genes related to tumor/immune-cell interactions was analyzed in diagnostic cHL biopsies to derive 22 signatures representing immune cell subtypes and programs, reconstructing the cHL microenvironment.[47] Unsupervised clustering revealed 2 main classes: one (52% of cases) dominated by macrophages, myeloid cells, stromal signatures, and cytokines,[48] and the other (48%) dominated by T-cell, B-cell, and immune checkpoint signatures (Figure 5A). Supervised digital deconvolution[49] confirmed higher macrophage and T-cell presence in each class, respectively (Figure 5C-E). Immunohistochemical analysis orthogonally validated these findings and consistently identified one group enriched in macrophage markers and another in T-cell markers among cases lacking gene expression data (Figure 5B). Expectedly, patients with a tumor microenvironment enriched in macrophages exhibited higher plasma levels of the macrophage-derived interleukin 1A and CCL22/MDC (Figure 5F). EBV infection and genetic features were evenly distributed across microenvironmental classes (supplemental Figure 21A).

Individual patient 3-digit HLA genotype and nonsynonymous ctDNA mutations were combined to predict neoantigens.[50] Only neoantigens from genes expressed in GC B cells and

Figure 2 (continued) cHL (N = 280). (C) The histogram shows the prevalence of mutations within a 20-bp window starting at individual nucleotide of the *BCL6* intron 1 in cHL (N = 280). The dashed lines delimitate hotspots. The horizontal line marks the genomic coordinate (hg19). (D) ChIP-Seq tracks, H3K27Ac at the *BCL6* intron 1 region in normal GC B cells and cHL cell lines annotated for mutation status at hotspot 7 and expression status of BCL6. Enrichment is visualized as reads per bins per million bps (BPM), and the genomic coordinates of the region shown (hg19) are provided at the bottom. Red horizontal bars below the H3K27Ac tracks indicate regions identified as SE by ROSE. The yellow bar indicates the hypermutated region of *BCL6* Hotspot 7. (E) Histogram of the mean H3K27ac signal intensity in wild-type vs mutated cHL cell lines at the hotspot 7 position. M, mutated; WT, wild type.

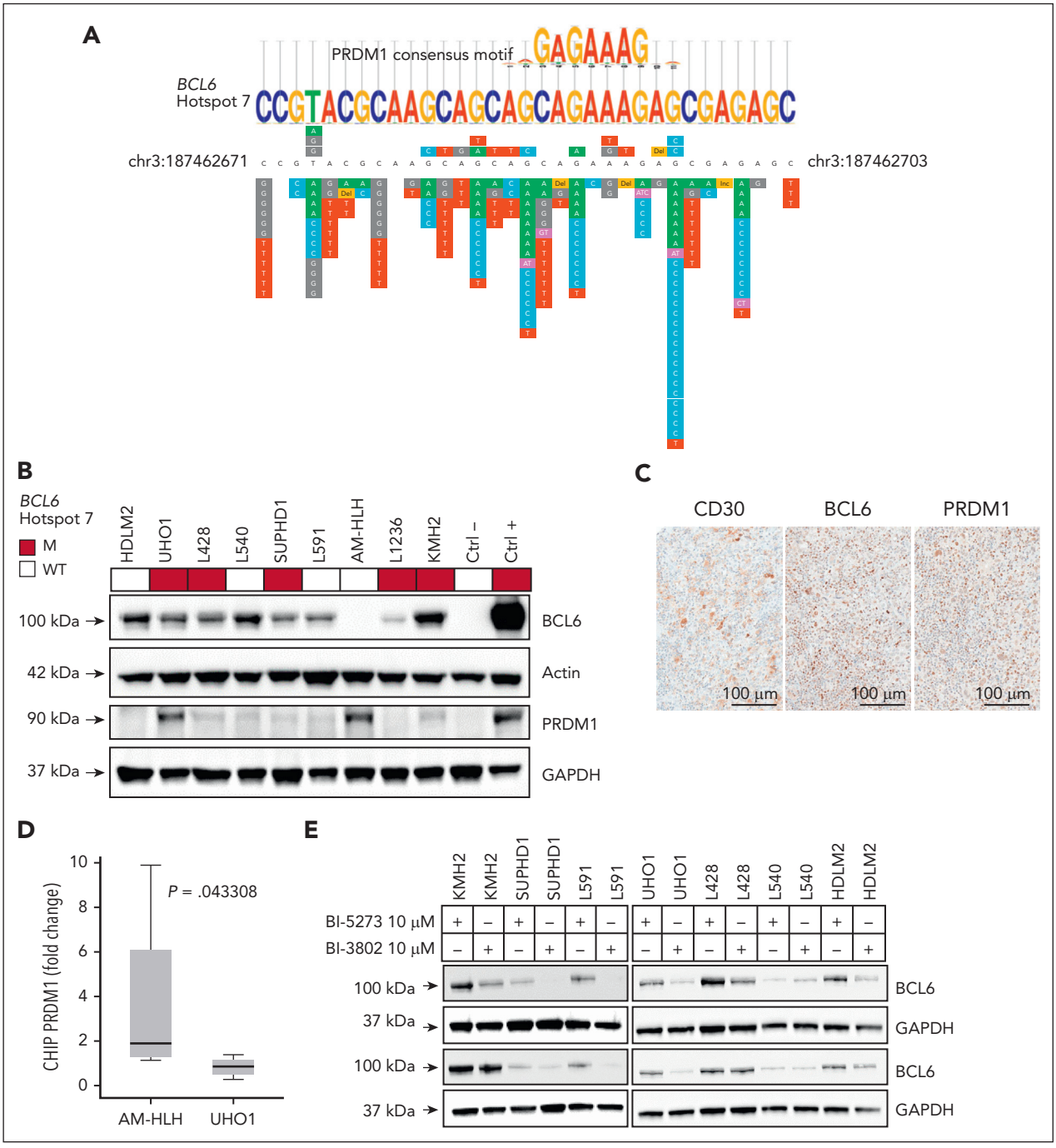

Figure 3. *BCL6* hotspot 7 mutations. (A) Magnified view of the *BCL6* mutational hotspot 7 at single-nucleotide resolution, with the mutations identified in patients with cHL aligned to the RefSeq (cHL cell lines above, patients with cHL below; genomic coordinate in hg19). The PRDM1 consensus motif identified by Tomtom within databases of known motifs is aligned above the RefSeq. (B) Western blot analysis of BCL6 and PRDM1 protein expression in cHL cell lines carrying wild-type or aberrant *BCL6* hotspot 7 (color coded as indicated). For BCL6: the positive control is the *BCL6*-translocated SUDHL4 DLBCL cell line and the negative control is the Toledo DLBCL cell line. Actin control for total protein loading. For PRDM1: the positive control is the U266 multiple myeloma cell line and the negative control is the SUDHL4 DLBCL cell line. GAPDH control for total protein loading. (C) TMA sections stained with anti-BCL6, anti-PRDM1, and anti-CD30 to highlight HRS cells and representing an illustrative cHL case with *BCL6* hotspot 7 mutation that coexpresses BCL6 and PRDM1. (D) PRDM1 ChIP-qPCR in the AM-HLH cell line that expresses PRDM1 and is wild type in *BCL6* hotspot 7, and in the UHO1 cell line that expresses PRDM1 and is mutated in *BCL6* hotspot 7 (n = 2 technical replicates pooled from 4 independent experiments). Box plot showing the median (the number within the box), quartiles, 95% percentiles, and extremes of fold enrichment against IgG. (E) Western blot showing the expression levels of BCL6 in cHL cell lines treated with BI-3802 or the analogue molecule BI-5273 for 7 days (2 biological replicates). SUPHD1, L591, UHO1, and HDLM2 showed BCL6 protein degradation. GAPDH was used as a loading control. (F) Volcano plots of differential gene expression comparing cell lines treated with the BCL6 degrader BI-3802 vs the BI-5372 control molecule. cHL cell lines that showed BCL6 protein degradation are reported along with the SUDHL4 (*BCL6*-translocated DLBCL) control cell line. Blue dots indicate significantly down-regulated genes ($P < .05$, log2 FC < 0), red dots indicate significantly upregulated genes ($P < .05$, log2 FC > 0). Highlighted are upregulated BCL6 targets.[37] Cell lines treated with 10 µM BI-3802 or the analogue molecule BI-5273 for 7 days (2 biological replicates). (G) The bar graph illustrates the proliferation rates of SUDHL4 and 7 cHL cell lines expressing BCL6 under BCL6 degrader BI-3802 and analogue BI-5273. Each pair of bars represents a different cell line. Within each pair, bars show the duration of treatment (day 3 and day 7). Cells were treated with BI-3802 and BI-5273 at 10 µM and incubated for the indicated times. Proliferation rates were measured using BrdU incorporation assay and normalized to the control condition (cells treated with the analogue molecule BI-5273). Data are averaged from 3 independent experiments. Statistical significance was determined using a paired *t*-test. *$P < .05$; **$P < .01$; ***$P < .001$.

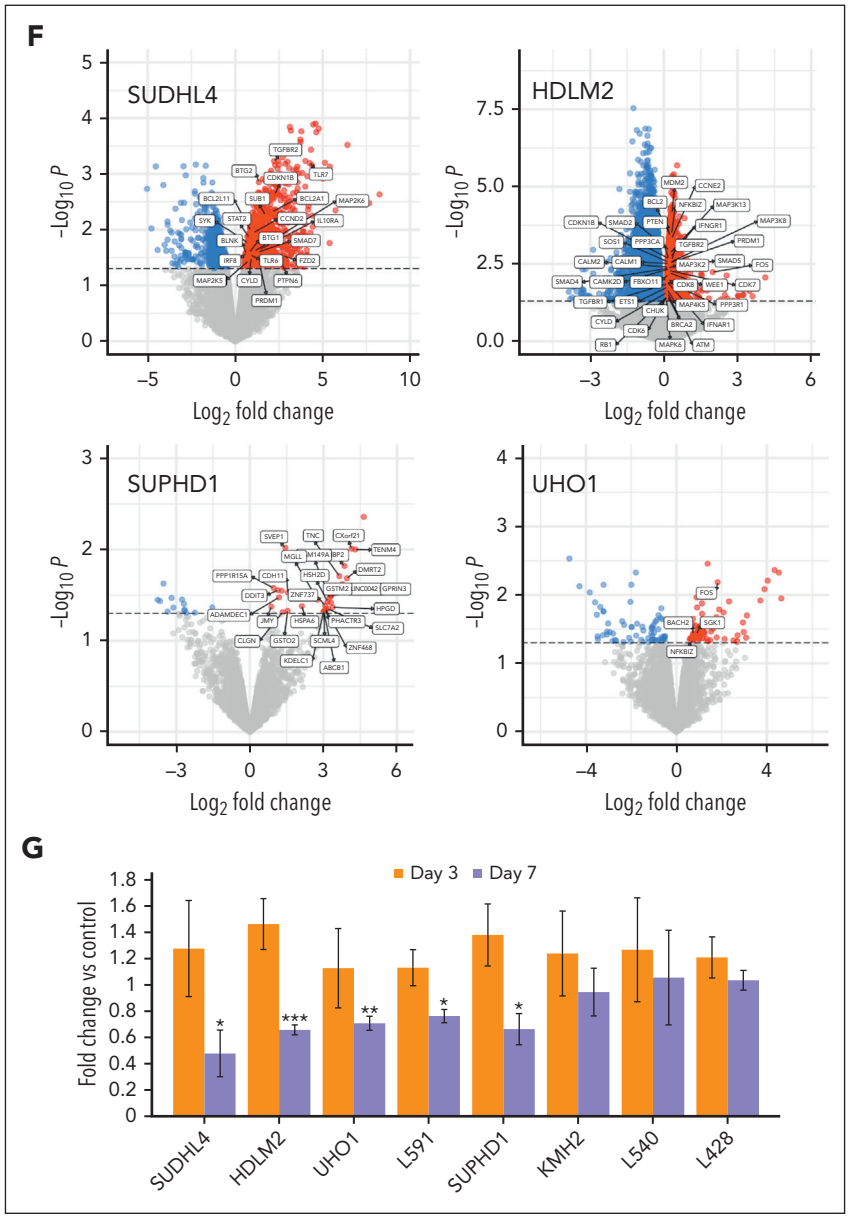

Figure 3 (continued)

GC-derived B-cell lymphoma cell lines were considered. For validation and in line with previous reports, this approach identified an average of 4 predicted neoantigens (ranging from 0 to 18) when applied to DLBCL samples (n = 29).[50] In cHL, we identified an average of 3 predicted neoantigens (range, 0-32). The number of predicted neoantigens was higher in cHL cases with a macrophage-enriched microenvironment than in patients with a T-cell enriched microenvironment (Figure 5G), consistent with the selective pressure exerted by T cells on the tumor.[51,52]

Levels of 71 cytokines/chemokines were measured in pretreatment plasma, and patients were unsupervisedly clustered into 2 distinct patterns based on their predicted cytokine/chemokine profiles (supplemental Figure 22A). Pattern 1 (26% of cases) showed elevated levels of cytokines and chemokines linked to T follicular helper cells and had an enrichment PD1$^+$/CXCL13$^+$ cells surrounding HRS cells (supplemental Figure 22C-E).[53] Pattern 2 had a nonspecific profile. Genetic alterations, EBV infection, and neoantigen numbers were similar across both patterns (supplemental Figures 21B and 22B). Cytokines, cytokine patterns, and tumor microenvironment classes showed no correlation with genetic subtypes (supplemental Figure 23A). Cytokines and cytokine patterns were also distributed without significant differences across the microenvironment classes (supplemental Figure 23B).

Together, these findings suggest that the predicted neoantigen load, rather than specific genetic alterations, shapes the microenvironment of cHL. The cytokine deregulation observed in cHL cannot be linked to any known genetic mechanism associated with the disease.

Table 2. Univariate analysis of PFS

Treatment-naïve IOSI-EMA003	HR	95% CI	*P*
Age (continuous)	1.026	1.008-1.044	.004693
Male	0.781	0.421-1.447	.431562
ECOG PS >1	5.275	2.430-11.454	.000026
Histology			
Mixed cellularity	—	—	—
Nodular sclerosis	0.868	0.337-2.239	.770232
Other	0.898	0.274-2.944	.859143
Ann Arbor stage III-IV	1.5	0.800-2.182	.206304
IPS >2	4.017	2.124-7.598	.000019
B symptoms	4.037	1.976-8.245	.000128
Large mediastinal mass	1.696	0.877-3.279	.116225
Extranodal involvement	1.375	0.742-2.548	.311846
≥3 Nodal areas	1.124	0.498-2.537	.778003
Elevated ESR	2.938	1.548-5.574	.000974
GHSG stage	2.271	1.209-4.265	.010779
EBV positivity	1.675	0.789-3.555	.179061
MTV (continuous)	1.001	1.001-1.002	.000985
iPET	4.649	2.435-8.874	.000003

CI, confidence interval; ESR, erythrocyte sedimentation rate; GHSG, German Hodgkin Study Group; HR, hazard ratio; iPET, interim PET/CT; IPS, International Prognostic Score; MTV, metabolic tumor volume.

Neoantigen clonality and response to immune checkpoint blockade

In solid cancers, the clinical effectiveness of checkpoint inhibitors is linked to the tumor's clonal structure, as subclonal neoantigens are less effective than clonal neoantigens in engaging immune surveillance—specifically, the neoantigen clonal structure is considered more predictive of response to checkpoint inhibitors and prognosis than the total number of neoantigens.[54-57] The impact on antitumor response of neoantigen clonality was assessed in 35 relapsed/refractory cHL treated with checkpoint inhibitors, and, for comparative purposes, in therapy-naïve patients who received chemotherapy (Table 1). Patients with predicted neoantigens arising from subclonal mutations had shorter PFS when treated with checkpoint inhibitors compared with those with only clonal neoantigens (Figure 6A). Conversely, the presence of subclonal neoantigens did not impact PFS following chemotherapy (Figure 6B), as this treatment does not depend on T-cell engagement. The total number of neoantigens (HR, 1.02; 95% CI, 0.93–1.12; $P = .612507$) and the ratio of neoantigens to the total number of mutations (HR, 3.57; 95% CI, 0.17–109.50; $P = .465889$) showed no correlation with PFS following checkpoint inhibitor treatment. This aligns with the concept that intratumoral heterogeneity of neoantigens is a stronger predictor of response to checkpoint inhibitors and prognosis than the total neoantigen count.[54-56]

After 3 to 6 months of checkpoint inhibitor therapy, the majority (79%) of the pretreatment predicted neoantigens were no longer detectable in ctDNA of responding patients, and few new neoantigens were gained (Figure 6C,E). In contrast, ctDNA that persisted after chemotherapy either lost or gained mutations that predicted neoantigens (Figure 6D,F).

These findings indicate that neoantigen clonality is a prognosticator of therapeutic response to checkpoint inhibitors, and that the evolution of neoantigens during checkpoint inhibitor treatment follows the process of immune editing.[57]

Molecular response in prognosticating treatment outcome

Although our selector targeted genomic regions known to be enriched in recurrent phased variants of lymphomas, we opted to use the CAPP-seq[58] bioinformatics to assess the molecular response in cHL, despite its lower sensitivity compared with phased variants bioinformatics.[59] This decision was based on the fact that 38% of patients with cHL did not have ctDNA molecules that supported phased variants in the pretreatment plasma, whereas, as previously reported,[59] we detected phased variants in most DLBCL cases. These observations suggest that phased variants are less effective for monitoring molecular response in cHL (supplemental Figure 24).

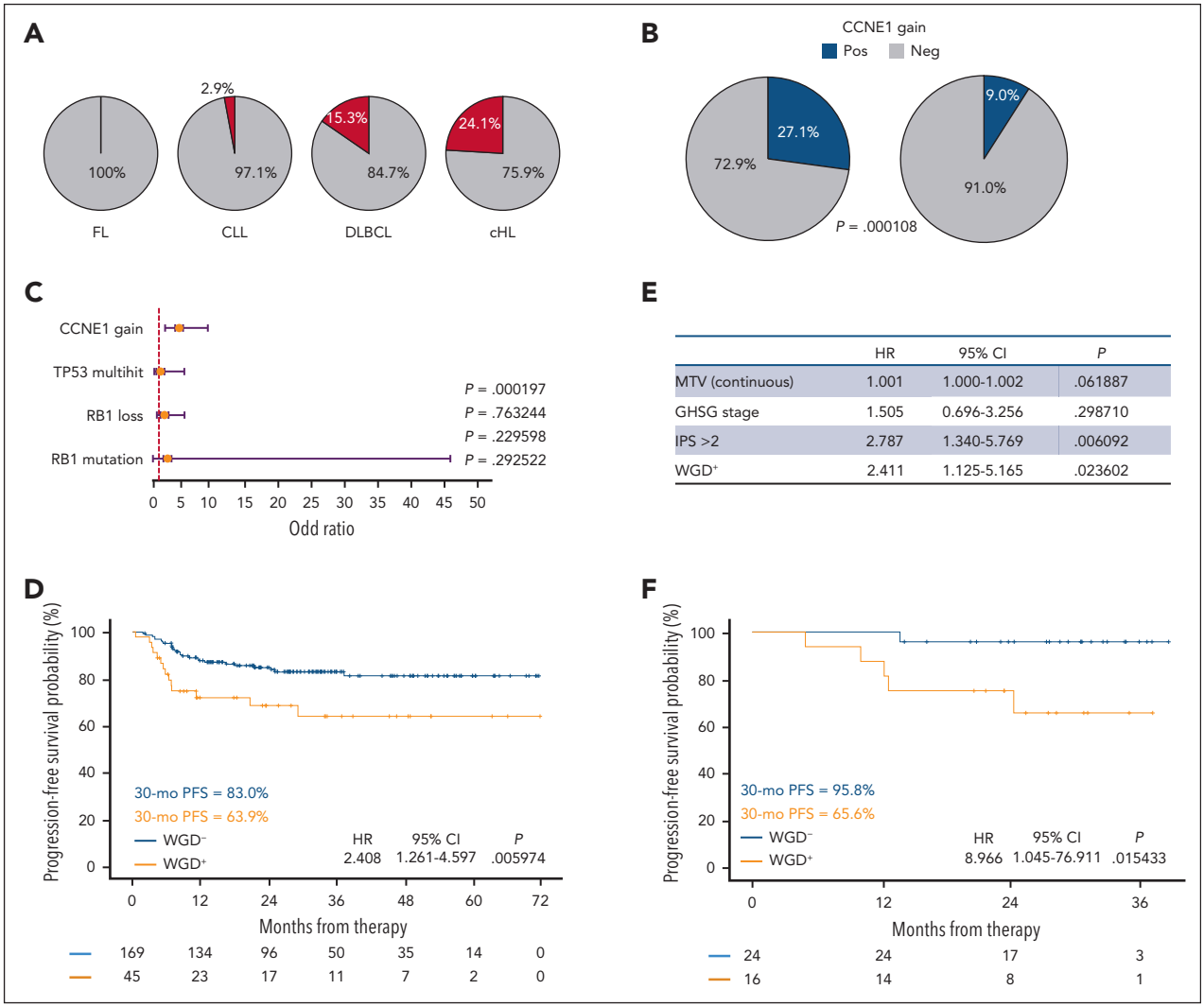

Figure 4. Whole-genome doubling in cHL and clinical correlations. (A) Pie charts showing the prevalence of WGD among cases of FL (N = 8), CLL (N = 34, WGD$^+$ = 1, WGD$^-$ = 33), DLBCL (N = 39, WGD$^+$ = 6, WGD$^-$ = 33), and cHL (N = 291, WGD$^+$ = 70, WGD$^-$ = 221). (B) Pie charts showing the prevalence of *CCNE1* gain among cases of cHL with (N = 70) and without (N = 221) WGD. (C) Forest plot showing the univariate association (dot: odd ratio: whiskers: 95% CI) between WGD and genetic lesions of cHL that are known to associate with WGD. (D) Kaplan-Meier curve showing the cumulative PFS probabilities of patients with untreated cHL of the IOSI-EMA003 cohort stratified according to the presence (+) or absence (−) of WGD. Univariate hazard ratio (HR) and corresponding 95% confidence interval are shown. *P* value by log-rank test. (E) Multivariate Cox regression analysis for PFS of patients with untreated cHL of the IOSI-EMA003 cohort. (F) Kaplan-Meier curve showing the cumulative PFS probabilities of patients with untreated cHL of the FIL-RougeBIO cohort stratified according to the presence (+) or absence (−) of WGD. Univariate hazard ratio (HR) and corresponding 95% confidence interval are shown. *P* value by log-rank test.

All patients with ctDNA persistence at the interim (6% of cases) or end of treatment (16% of cases) time points showed no response or experienced rapid relapse (Figure 7A-B). The PFS of patients with positive interim and end-of-treatment PET/CT scans is also shown for comparative purposes (supplemental Figure 25). Bivariate analysis revealed that persistence of ctDNA is prognostic regardless of PET/CT at interim and end-of-treatment time points (Figure 7C-D). Patients with positive interim or end-of-therapy PET/CT results but without detectable ctDNA exhibited a PFS comparable to that of patients who tested negative on both PET/CT and ctDNA (supplemental Figure 26). Conversely, all patients who tested positive on both PET/CT and ctDNA eventually relapsed. Therefore, the detection of residual disease by ctDNA demonstrated a higher positive predictive value to that of PET/CT for PFS events, and an akin negative predictive value (Figure 7E-F).

Together, these data indicate that ctDNA may serve as a surrogate for tissue biopsy to verify tumor persistence in patients who show positive PET/CT results.

Discussion

By leveraging ctDNA, we present an overview of the genetic landscape of cHL and its connection to disease pathophysiology. Genomic clustering studies, including ours, identified cHL subsets distinguished by different mutation and SCNA loads.[5,7] However, unlike DLBCL,[60] where independent investigators have consistently identified molecular subgroups defined by the same genetic lesions, molecular subtypes of cHL showed little overlap in genetic abnormalities across studies.[5,7] These discrepancies can be explained by our finding that, much like in colorectal cancer,[61] the mechanism of genetic instability

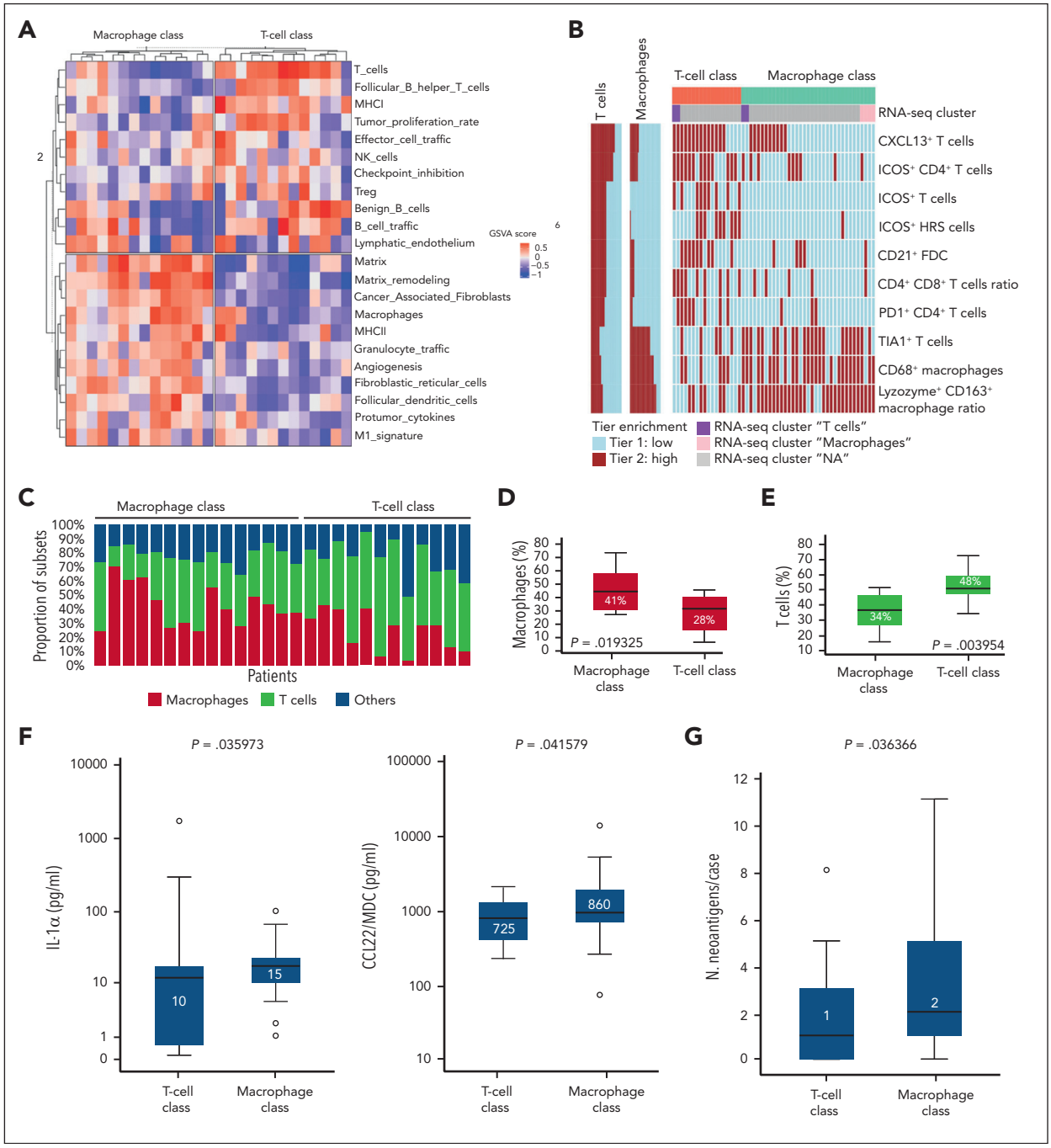

Figure 5. Immune microenvironment. (A) Heat map of scaled activity score values related to microenvironment signatures by bulk RNA sequencing (RNA-seq) of diagnostic tissue biopsies (N = 27) from untreated patients with cHL. Each column represents a sample, and signatures are represented in rows. Unsupervised clustering reveals 2 classes named "macrophage" and "T-cell" according to their gene signatures. (B) Heat map shows the expression of significant cell type–defining antigens by TMA of diagnostic tissue biopsies (N = 53) from untreated patients with cHL. Each column represents a sample, and protein markers are represented in rows. Color codes indicate the expression score (tier). Unsupervised clustering based on the expression scores reveals 2 classes named macrophage and T-cell according to the cell composition of the microenvironment. Cases for which both gene expression and TMA were available (N = 8) are annotated in the header. (C) Stacked bar plots represent the individual cell compositions (scaled to a total of 100%) by digital cytometry. Bulk RNA-seq data of diagnostic tissue biopsies (N = 27) from untreated patients with cHL are used to infer the cell composition (macrophage and T-cell subtypes are consolidated, others indicate cells other than macrophages and T cells). Samples (on the x-axis) are ordered by supervised clustering into macrophage and T-cell classes. (D) Box plot showing the median (the number within the box), quartiles, 95% percentiles, and extremes of the macrophage percentage inferred by digital cytometry in tissue biopsies belonging to the macrophage class (n = 14) and T-cell class (n = 13), respectively. *P* values determined by Mann-Whitney test. (E) Box plot showing the median (the number within the box), quartiles, 95% percentiles, and extremes of the T-cell percentage inferred by digital cytometry in tissue biopsies belonging to the macrophage class (n = 14) and T-cell class (n = 13), respectively. *P* values determined by Mann-Whitney test. (F) Box plot showing the median (the number within the box), quartiles, 95% percentiles, and extremes of the plasma levels of cytokines that differed between patients of the T-cell (N = 24) and macrophage (N = 38) classes. *P* values determined by Mann-Whitney test. (G) Box plot showing the median (the number within the box), quartiles, 95% percentiles, and extremes of the number of predicted neoantigens per case in patients of the T-cell (N = 20) and macrophage (N = 34) classes. *P* values determined by Mann-Whitney test. MDC, macrophage-derived chemokine; MHC, major histocompatibility complex; NK, natural killer.

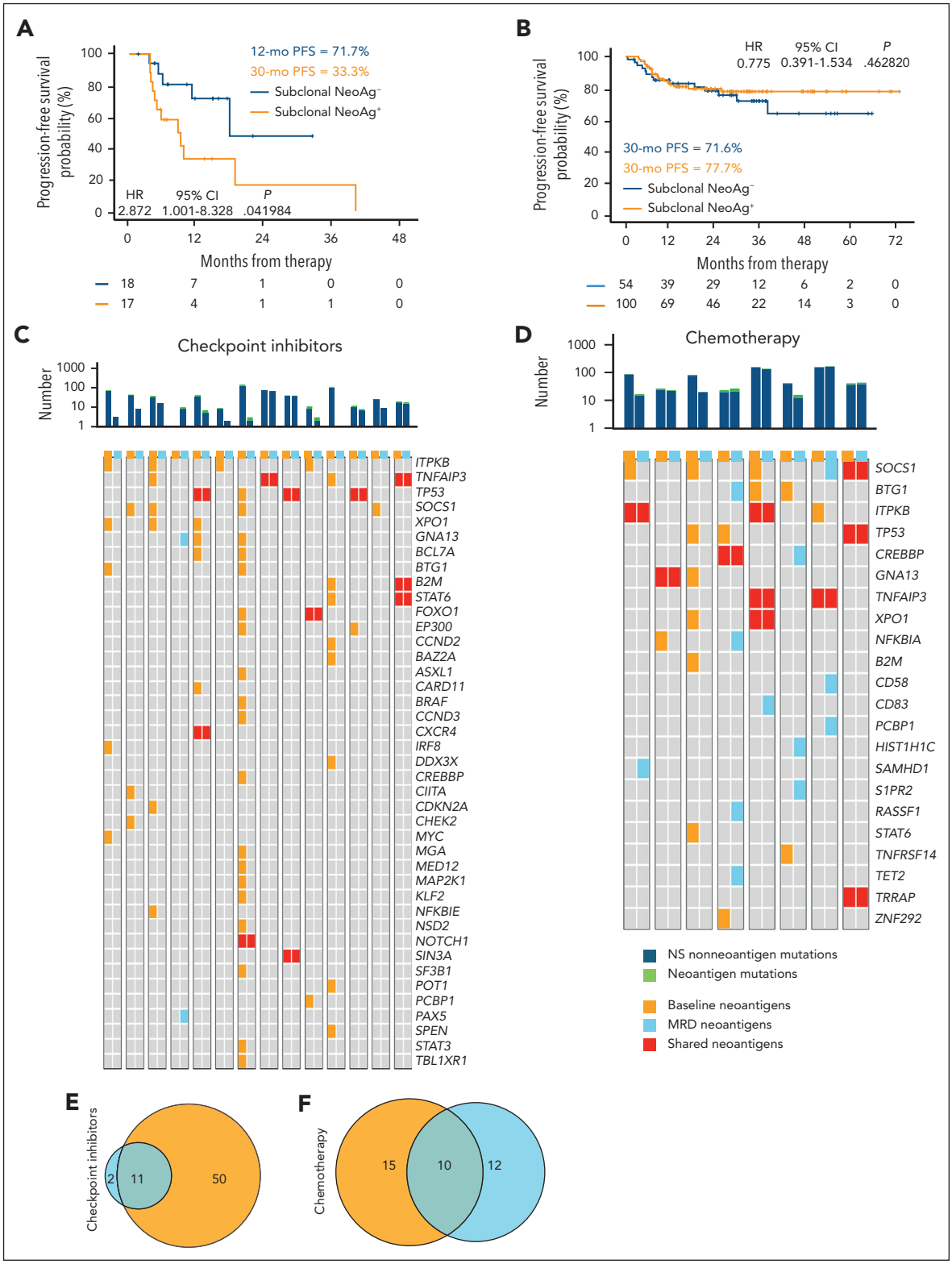

Figure 6. Predicted neoantigens in cHL and their association with PFS and treatment response. (A) Kaplan-Meier curve showing the cumulative PFS probabilities of patients with relapsed/refractory cHL of the IOSI-EMA003 cohort treated with checkpoint inhibitors and stratified according to the presence (+) or absence (−) of subclonal predicted neoantigens. Univariate hazard ratio (HR) and corresponding 95% confidence interval are shown. *P* value by log-rank test. (B) Kaplan-Meier curve showing the cumulative PFS probabilities of patients with untreated cHL of the IOSI-EMA003 cohort stratified according to the presence (+) or absence (−) of subclonal predicted neoantigens. Univariate HR and corresponding 95% confidence interval are shown. *P* value by log-rank test. Oncoprint showing the evolution of predicted neoantigens under treatment with checkpoint inhibitors (C) or chemotherapy (D). Each paired column is a patient. Color codes of the headers of each column show the time point of the assessment. Cells are color coded according to the evolution of neoantigens (yellow, predicted neoantigens that were observed in the pretreatment ctDNA but not in the residual ctDNA persisting after 3-6 months of treatment with checkpoint inhibitors or at the end of chemotherapy; blue, predicted neoantigens that were observed only in the residual ctDNA persisting after 3-6 months of treatment with checkpoint inhibitors or at the end of chemotherapy, but not in the pretreatment ctDNA; red, predicted

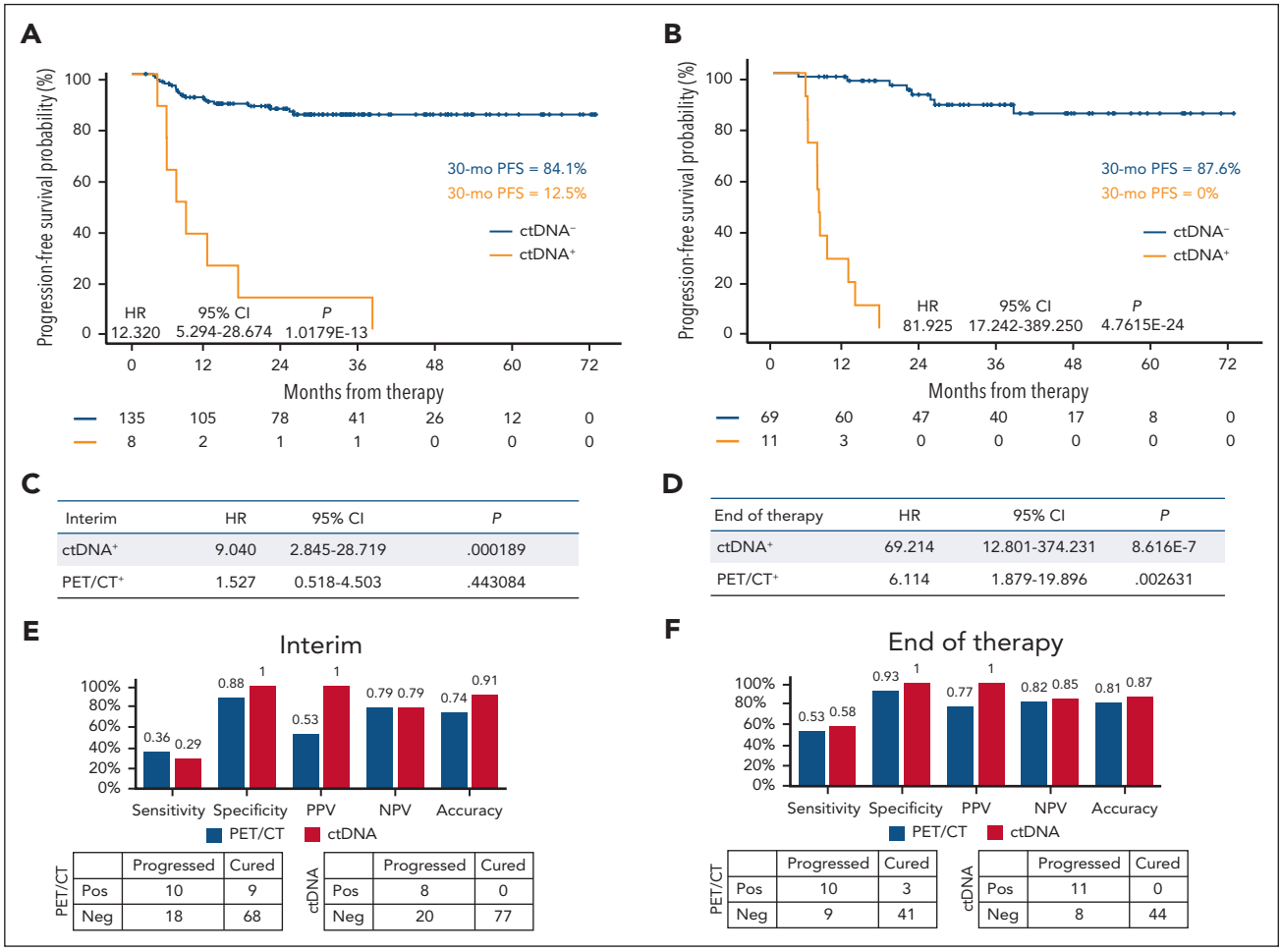

Interim	HR	95% CI	P
ctDNA⁺	9.040	2.845-28.719	.000189
PET/CT⁺	1.527	0.518-4.503	.443084

End of therapy	HR	95% CI	P
ctDNA⁺	69.214	12.801-374.231	8.616E-7
PET/CT⁺	6.114	1.879-19.896	.002631

PET/CT	Progressed	Cured
Pos	10	9
Neg	18	68

ctDNA	Progressed	Cured
Pos	8	0
Neg	20	77

PET/CT	Progressed	Cured
Pos	10	3
Neg	9	41

ctDNA	Progressed	Cured
Pos	11	0
Neg	8	44

Figure 7. PFS according to interim and end-of-therapy molecular response. Kaplan-Meier curve showing the cumulative PFS probabilities of patients with untreated intermediate-advanced stage cHL of the TN IOSI-EMA003 cohort. Patients are stratified for (A) interim ctDNA levels and (B) end-of-treatment ctDNA levels (ctDNA$^-$ = absence; ctDNA$^+$ = persistence). Univariate hazard ratio (HR) and corresponding 95% confidence interval are shown. *P* value by log-rank test. Bivariate Cox regression for PFS of intermediate-advanced cHL of the TN IOSI-EMA003 cohort; HR and corresponding 95% confidence interval are shown for interim (C) and end-of-treatment (D) time points. PET$^+$ = DS4-5; ctDNA$^+$ = persistence. Bar plot showing the diagnostic performance parameters of PET/CT and ctDNA at the interim (E) and end-of-treatment (F) time points of patients with untreated intermediate-advanced cHL of the TN IOSI-EMA003 cohort. The analysis includes patients who had PFS events and censored patients with at least 24 months of follow-up. The table below the graph shows the diagnostic test results vs the gold standard (progressed or cured). NPV, negative predictive value; PPV, positive predictive value.

underlying each case is the primary factor driving the genetic subtypes of cHL, rather than the grouping of mutations into functional categories. The C1 subgroup is hypermutated with a contribution of both AID and MSI signatures, whereas the C2 subgroup exhibits high levels of chromosomal instability. In line with our observations, the SBS84 AID signature has been already reported in a fraction of cHL,[3,4] MSI is a characteristic of several cHL cell lines,[62] and defects of mismatch repair have been described in hypermutated cHL.[3,6]

Noncoding regulatory mutations are a characteristic feature of DLBCL among B-cell non-Hodgkin lymphomas.[14] Using our targeted approach informed by current knowledge of B-cell lymphoma genetics, we discovered that cHL shares this molecular mechanism with DLBCL and highlight genetic lesions in the noncoding genome as a previously overlooked aspect of cHL biology. This finding prompts whole-genome studies aimed at uncovering unexpected noncoding seQTL, as the causes of the extensive reshaping of the GC B-cell program that characterizes HRS cells[63] remain enigmatic and cannot be explained by mutations in the coding genome.

Disruption of the program that regulates GC B-cell differentiation into plasma cells is a feature of cHL.[64] Both BCL6 and PRDM1 are crucial for this program: BCL6 maintains B cells in the GC, whereas PRDM1 promotes plasma cell differentiation by suppressing BCL6 transcription.[65] Noncoding regulatory mutations of *BCL6* can contribute to the disruption of this differentiation process. cHL has the same seQTL of the *BCL6*-intragenic SE (that we named hotspot 7) found in DLBCL.[14]

Figure 6 (continued) neoantigens that were observed in both pretreatment ctDNA and residual ctDNA persisting after 3-6 months of treatment with checkpoint inhibitors or at the end of chemotherapy). The bar graph on top of the oncoprint shows the number of nonsynonymous mutations, including those that predicted neoantigens and those that did not. Venn diagrams showing how many predicted neoantigens were shared between pretreatment and residual ctDNA in patients treated with checkpoint inhibitors (E) or chemotherapy (F). MRD, measurable residual disease.

Similar to DLBCL, the seQTL of *BCL6* in cHL hinders PRDM1 binding to *BCL6*, and can contribute to BCL6 expression in a fraction of cHL. At the molecular level, the observation that BCL6 degradation in cHL results in the derepression of BCL6-regulated genes suggests that BCL6 plays a functional role in orchestrating, at least in part, the aberrant gene expression program of cHL. At the cellular level, the finding that cHL shows reduced proliferation following BCL6 degradation highlights the role of BCL6 in sustaining this tumor and might have therapeutic implications, as BCL6 degraders are being investigated for their efficacy and safety clinical studies as potential treatments for BCL6-dependent lymphomas.

WGD is associated with a lower chance of cure following initial cHL treatment. It is common in cHL and strongly linked to *CCNE1* gain, which is notable because cyclin E overexpression is prevalent and specific to cHL among B-cell lymphomas.[1,66,67] In solid cancers, cyclin E overexpression disrupts the TP53 checkpoint, enabling endoreplication even with functional TP53.[43] Collectively, these notions offer insights into the pathophysiology behind the giant Hodgkin cells and the multinucleated Reed-Sternberg cells, which result from endoreduplication or cytokinesis errors causing the fusion of daughter cells, even in the presence of intact *TP53*.[41,68] Beyond being a genetic feature and a prognostic indicator in cHL, WGD may also hold therapeutic significance, especially because cancers that rely on cyclin E for WGD might be susceptible to cyclin-dependent kinase 2 inhibitors.[69] The frequent overexpression of cyclin E in cHL cannot be entirely attributed to *CCNE1* gain alone. Given the role of noncoding regulatory mutations in cHL, further investigation is needed to determine whether cyclin E overexpression is driven by a deregulated program induced by these regulatory mutations.

By identifying cancer-specific markers, ctDNA offers greater positive predictive value than PET/CT in detecting persistent disease during and after treatment. Consequently, the clinical utility of ctDNA in cHL is to differentiate between ambiguous PET/CT-positive lesions that remain despite treatment. This application is bolstered by the minimally invasive nature of liquid biopsy. Persistent small focal lesions detected by PET/CT are often unrelated to the tumor in a significant number of patients, as PET/CT can also capture the metabolic activity of noncancerous, inflammatory tissues. Such findings frequently complicate management by prompting further medical interventions, including invasive biopsies, additional PET/CT scans, and potentially unnecessary application of consolidation radiotherapy or intensified chemotherapy. The clinical utility of ctDNA monitoring in cHL using CAPP-seq is currently being prospectively validated in the RAFTING trial (NCT04866654).

Acknowledgments

This study was supported by European Research Council Consolidator grant 772051; Swiss Cancer Research Foundation grants 3746, 4395, 4660, 5257, and 5778; Swiss National Science Foundation grants 320030_169670/1, 310030_192439, 320036_179318, 320030_228064, and 320030_220238; Leukemia & Lymphoma Society grant 6594-20; the CLL Global Foundation; the ISREC Foundation; the Helmut Horten Foundation; the Nelia & Amadeo Barletta Foundation; the Fond'Action; Fondazione Ticinese per la Ricerca sul Cancro; the Jacques & Gloria Gossweiler Foundation; the ETH Lymphoma Challenge; the ASH Global Award; the Area Formazione, Ricerca e Innovazione Ente Ospedaliero Cantonale; the Associazione "l'Albero dei Sorrisi"-ONLUS; the Swiss Group for Clinical Cancer Research 38/19; and the Italian Association for Cancer Research grant 20575.

Authorship

Contribution: D.R. designed the study, interpreted data, and wrote the manuscript; M.C.P. managed the study, curated the clinical database, performed statistical analysis, and contributed to the study design and manuscript preparation; A.B. designed CAPP-seq experiments and interpreted the data; L.T.d.B. and M.S. implemented the bioinformatic analysis and contributed to manuscript preparation; S.B., G.A.G., K.P., V.S., and C.G. managed the study biobank, prepared the study samples, and performed next-generation sequencing experiments; D.P. performed chromatin immunoprecipitation assays and interpreted the results; G.F. performed in vitro studies and interpreted the results; G.F. and A.R. performed RNA-sequencing experiments and ATAC-seq experiments; F.J. and A.T. reviewed histologies, designed and performed tissue microarrays, and contributed to data interpretation and formulation of research goals; A.C. and I.R. curated the clinical database and contributed to data interpretation and formulation of research goals; S.A., P.B., E.C., S.C., F.C., R.D.F., B.G., M.K., M.d.T., V.C., R.M., A. Stathis, G.S., I.Z., and A.P. collected clinical data and provided study samples; E.M., R.B., L.M.L., and L.M. performed pathology analyses; F.B., E.B., S.C., M.C., M.R., G.R., G.M.S., and L.C. centrally revised positron emission tomography/computed tomography images; V.G., J.M.Z., A. Santoro, S.H., F.C., and C.C.-S. contributed to the formulation of overarching research goals and to data interpretation; and L.C., G.G., and E.Z. contributed to the formulation of overarching research goals, and to the study design, data interpretation, and manuscript preparation.

Conflict-of-interest disclosure: M.C.P. has received travel grants from BeiGene and Janssen. A.C. has received honoraria from AbbVie, AstraZeneca, BeiGene, and Janssen and research funding from Gilead and Pfizer. E.Z. received research funding from AstraZeneca, BeiGene, Celgene/Bristol Myers Squibb, Incyte, Janssen, and Roche; honoraria from AbbVie, BeiGene, Bristol Myers Squibb, Curis, Eli/Lilly, Incyte, Ipsen, Merck, Miltenyi Biomedicine, and Roche; and travel grants from AstraZeneca, BeiGene, Janssen, and Gilead. A. Stathis has received research funding from AbbVie, ADC Therapeutics, Amgen, AstraZeneca, Bayer, Bristol Myers Squibb, Cellestia, Incyte, Loxo Oncology, Merck MSD, Novartis, Pfizer, Philogen, Prelude Therapeutics, and Roche; honoraria from Debiopharm, Janssen, AstraZeneca, Incyte, Eli Lilly, Novartis, Roche, and Loxo Oncology; and travel grants from Incyte and AstraZeneca. G.S. has received honoraria from AbbVie, Novartis, Bristol Myers Squibb, Gilead, Incyte, and Roche. G.G. has received honoraria from AbbVie, AstraZeneca, BeiGene, Hikma, Incyte, Janssen, and Lilly. C.C.-S. has received honoraria from Sanofi, ADC Therapeutics, Roche, AstraZeneca, Celgene/Bristol Myers Squibb, Incyte, Janssen Oncology, Takeda, Novartis, Gilead, SOBI, Merck Sharp & Dohme, Karyopharm Therapeutics, Scenic Biotech, AbbVie, and Genmab and research funding ADC Therapeutics, Roche, and Sanofi. S.H. has received honoraria from BeiGene, Bristol Myers Squibb, Gilead, Lilly, Incyte, Ipsen, Novartis, Roche, and Takeda. A. Santoro has received honoraria from Sanofi, Incyte, Bristol Myers Squibb, Servier, Gilead, Pfizer, EISAI, Bayer, MSD, Takeda, Roche, AbbVie, Amgen, Celgene, AstraZeneca, Arqule, Lilly, Sandoz, Novartis, and BeiGene. D.R. has received honoraria from AbbVie, AstraZeneca, BeiGene, Bristol Myers Squibb, and Janssen; research grants from AbbVie, AstraZeneca, and Janssen; and travel grants from AstraZeneca and Janssen. The remaining authors declare no competing financial interests.

ORCID profiles: A.B., 0009-0004-9938-0396; R.M., 0000-0001-7393-1138; V.C., 0000-0001-7345-3383; I.R., 0000-0001-5720-9807; E.B., 0000-0001-8655-2743; S. Chauvie, 0000-0003-4394-5031; S. Crisci, 0000-0002-0567-2709; M.C., 0000-0002-8214-562X; R.D.F., 0000-0001-7899-3071; B.G., 0000-0001-5418-0949; M.K., 0000-0002-6134-7425; G.M.S., 0000-0003-2690-4078; I.Z., 0000-0002-8168-7398; A.P., 0000-0002-9425-9026; J.M.Z., 0000-0002-0986-8936; A. Santoro, 0000-0003-1709-9492; S.H., 0000-0002-5534-7197; C.C., 0000-0003-3144-0124; G.G., 0000-0002-4681-0151; L.C., 0000-0002-6371-097X.

Correspondence: Davide Rossi, Institute of Oncology Research, 6500 Bellinzona, Switzerland; email: davide.rossi@eoc.ch.

Footnotes

Submitted 23 October 2024; accepted 10 April 2025; prepublished online on *Blood* First Edition 13 May 2025. https://doi.org/10.1182/blood.2024027355.

*M.C.P., A.B., L.T.d.B., and MS. contributed equally to this study.

†G.G., L.C., E.Z., and D.R. contributed equally to this study.

Raw data used in this study have been deposited at EGA, under the accession number EGAS50000000873.

The online version of this article contains a data supplement.

There is a *Blood* Commentary on this article in this issue.

The publication costs of this article were defrayed in part by page charge payment. Therefore, and solely to indicate this fact, this article is hereby marked "advertisement" in accordance with 18 USC section 1734.

REFERENCES

1. Tiacci E, Ladewig E, Schiavoni G, et al. Pervasive mutations of JAK-STAT pathway genes in classical Hodgkin lymphoma. *Blood*. 2018;131(22):2454-2465.
2. Reichel J, Chadburn A, Rubinstein PG, et al. Flow sorting and exome sequencing reveal the oncogenome of primary Hodgkin and Reed-Sternberg cells. *Blood*. 2015;125(7):1061-1072.
3. Wienand K, Chapuy B, Stewart C, et al. Genomic analyses of flow-sorted Hodgkin Reed-Sternberg cells reveal complementary mechanisms of immune evasion. *Blood Adv*. 2019;3(23):4065-4080.
4. Maura F, Ziccheddu B, Xiang JZ, et al. Molecular evolution of classic Hodgkin lymphoma revealed through whole-genome sequencing of Hodgkin and Reed Sternberg cells. *Blood Cancer Discov*. 2023;4(3):208-227.
5. Alig SK, Shahrokh Esfahani M, Garofalo A, et al. Distinct Hodgkin lymphoma subtypes defined by noninvasive genomic profiling. *Nature*. 2024;625(7996):778-787.
6. Gomez F, Fisk B, McMichael JF, et al. Ultra-deep sequencing reveals the mutational landscape of classical Hodgkin lymphoma. *Cancer Res Commun*. 2023;3(11):2312-2330.
7. Heger JM, Mammadova L, Mattlener J, et al. Circulating tumor DNA sequencing for biologic classification and individualized risk stratification in patients with Hodgkin lymphoma. *J Clin Oncol*. 2024;42(35):4218-4230.
8. Spina V, Bruscaggin A, Cuccaro A, et al. Circulating tumor DNA reveals genetics, clonal evolution, and residual disease in classical Hodgkin lymphoma. *Blood*. 2018;131(22):2413-2425.
9. Desch AK, Hartung K, Botzen A, et al. Genotyping circulating tumor DNA of pediatric Hodgkin lymphoma. *Leukemia*. 2020;34(1):151-166.
10. Sobesky S, Mammadova L, Cirillo M, et al. In-depth cell-free DNA sequencing reveals genomic landscape of Hodgkin's lymphoma and facilitates ultrasensitive residual disease detection. *Med*. 2021;2(10):1171-1193.e11.
11. Buedts L, Wlodarska I, Finalet-Ferreiro J, et al. The landscape of copy number variations in classical Hodgkin lymphoma: a joint KU Leuven and LYSA study on cell-free DNA. *Blood Adv*. 2021;5(7):1991-2002.
12. Camus V, Viennot M, Lequesne J, et al. Targeted genotyping of circulating tumor DNA for classical Hodgkin lymphoma monitoring: a prospective study. *Haematologica*. 2021;106(1):154-162.
13. Vandenberghe P, Wlodarska I, Tousseyn T, et al. Non-invasive detection of genomic imbalances in Hodgkin/Reed-Sternberg cells in early and advanced stage Hodgkin's lymphoma by sequencing of circulating cell-free DNA: a technical proof-of-principle study. *Lancet Haematol*. 2015;2(2):e55-e65.
14. Bal E, Kumar R, Hadigol M, et al. Super-enhancer hypermutation alters oncogene expression in B cell lymphoma. *Nature*. 2022;607(7920):808-815.
15. Shanbhag S, Ambinder RF. Hodgkin lymphoma: a review and update on recent progress. *CA Cancer J Clin*. 2018;68(2):116-132.
16. de Vries S, Schaapveld M, Janus CPM, et al. Long-term cause-specific mortality in Hodgkin lymphoma patients. *J Natl Cancer Inst*. 2021;113(6):760-769.
17. Eichenauer DA, Aleman BMP, André M, et al. Hodgkin lymphoma: ESMO Clinical Practice Guidelines for diagnosis, treatment and follow-up. *Ann Oncol*. 2018;29(suppl 4):iv19-iv29.
18. Adams HJA, Kwee TC. Proportion of false-positive lesions at interim and end-of-treatment FDG-PET in lymphoma as determined by histology: systematic review and meta-analysis. *Eur J Radiol*. 2016;85(11):1963-1970.
19. Barrington SF, Zwezerijnen B, de Vet HCW, et al. Automated segmentation of baseline metabolic total tumor burden in diffuse large B-cell lymphoma: which method is most successful? a study on behalf of the PETRA consortium. *J Nucl Med*. 2021;62(3):332-337.
20. Cheson BD, Fisher RI, Barrington SF, et al. Recommendations for initial evaluation, staging, and response assessment of Hodgkin and non-Hodgkin lymphoma: the Lugano classification. *J Clin Oncol*. 2014;32(27):3059-3068.
21. Pasqualucci L, Neumeister P, Goossens T, et al. Hypermutation of multiple proto-oncogenes in B-cell diffuse large-cell lymphomas. *Nature*. 2001;412(6844):341-346.
22. Khodabakhshi AH, Morin RD, Fejes AP, et al. Recurrent targets of aberrant somatic hypermutation in lymphoma. *Oncotarget*. 2012;3(11):1308-1319.
23. Hübschmann D, Kleinheinz K, Wagener R, et al. Mutational mechanisms shaping the coding and noncoding genome of germinal center derived B-cell lymphomas. *Leukemia*. 2021;35(7):2002-2016.
24. Bruscaggin A, Pini K, Rossi D. Detection of circulating tumor DNA in lymphoma patients. *Methods Mol Biol*. 2025;2865:475-490.
25. Bruscaggin A, di Bergamo LT, Spina V, et al. Circulating tumor DNA for comprehensive noninvasive monitoring of lymphoma treated with ibrutinib plus nivolumab. *Blood Adv*. 2021;5(22):4674-4685.
26. Talevich E, Shain AH, Botton T, Bastian BC. CNVkit: genome-wide copy number detection and visualization from targeted DNA sequencing. *PLoS Comput Biol*. 2016;12(4):e1004873.
27. Rothwell DG, Ayub M, Cook N, et al. Utility of ctDNA to support patient selection for early phase clinical trials: the TARGET study. *Nat Med*. 2019;25(5):738-743.
28. Esfahani MS, Hamilton EG, Mehrmohamadi M, et al. Inferring gene expression from cell-free DNA fragmentation profiles. *Nat Biotechnol*. 2022;40(4):585-597.
29. Hu ZY, Tang Y, Liu L, et al. Subtyping of metastatic breast cancer based on plasma circulating tumor DNA alterations: an observational, multicentre platform study. *EClinicalMedicine*. 2022;51:101567.
30. Lapin M, Edland KH, Tjensvoll K, et al. Comprehensive ctDNA measurements improve prediction of clinical outcomes and enable dynamic tracking of disease progression in advanced pancreatic cancer. *Clin Cancer Res*. 2023;29(7):1267-1278.
31. Adalsteinsson VA, Ha G, Freeman SS, et al. Scalable whole-exome sequencing of cell-free DNA reveals high concordance with metastatic tumors. *Nat Commun*. 2017;8(1):1324.
32. Cheson BD, Pfistner B, Juweid ME, et al. Revised response criteria for malignant lymphoma. *J Clin Oncol*. 2007;25(5):579-586.
33. Kanakry JA, Li H, Gellert LL, et al. Plasma Epstein-Barr virus DNA predicts outcome in advanced Hodgkin lymphoma: correlative analysis from a large North American cooperative group trial. *Blood*. 2013;121(18):3547-3553.
34. Schmitz R, Wright GW, Huang DW, et al. Genetics and pathogenesis of diffuse large B-cell lymphoma. *N Engl J Med*. 2018;378(15):1396-1407.
35. Chapuy B, Stewart C, Dunford AJ, et al. Molecular subtypes of diffuse large B cell lymphoma are associated with distinct

pathogenic mechanisms and outcomes. *Nat Med*. 2018;24(5):679-690.

36. Han X, Zhang S, Zhou DC, et al. MSIsensor-ct: microsatellite instability detection using cfDNA sequencing data. *Brief Bioinform*. 2021;22(5):bbaa402.

37. Basso K, Saito M, Sumazin P, et al. Integrated biochemical and computational approach identifies BCL6 direct target genes controlling multiple pathways in normal germinal center B cells. *Blood*. 2010;115(5):975-984.

38. Steidl C, Diepstra A, Lee T, et al. Gene expression profiling of microdissected Hodgkin Reed-Sternberg cells correlates with treatment outcome in classical Hodgkin lymphoma. *Blood*. 2012;120(17):3530-3540.

39. Słabicki M, Yoon H, Koeppel J, et al. Small-molecule-induced polymerization triggers degradation of BCL6. *Nature*. 2020;588(7836):164-168.

40. Kerres N, Steurer S, Schlager S, et al. Chemically induced degradation of the oncogenic transcription factor BCL6. *Cell Rep*. 2017;20(12):2860-2875.

41. Haber MM, Liu J, Knowles DM, Inghirami G. Determination of the DNA content of the Reed-Sternberg cell of Hodgkin's disease by image analysis. *Blood*. 1992;80(11):2851-2857.

42. Bielski CM, Zehir A, Penson AV, et al. Genome doubling shapes the evolution and prognosis of advanced cancers. *Nat Genet*. 2018;50(8):1189-1195.

43. Zeng J, Hills SA, Ozono E, Diffley JFX. Cyclin E-induced replicative stress drives p53-dependent whole-genome duplication. *Cell*. 2023;186(3):528-542.e14.

44. Hartmann S, Martin-Subero JI, Gesk S, et al. Detection of genomic imbalances in microdissected Hodgkin and Reed-Sternberg cells of classical Hodgkin's lymphoma by array-based comparative genomic hybridization. *Haematologica*. 2008;93(9):1318-1326.

45. Slovak ML, Bedell V, Hsu YH, et al. Molecular karyotypes of Hodgkin and Reed-Sternberg cells at disease onset reveal distinct copy number alterations in chemosensitive versus refractory Hodgkin lymphoma. *Clin Cancer Res*. 2011;17(10):3443-3454.

46. Roberts SA, Gordenin DA. Hypermutation in human cancer genomes: footprints and mechanisms. *Nat Rev Cancer*. 2014;14(12):786-800.

47. Kotlov N, Bagaev A, Revuelta MV, et al. Clinical and biological subtypes of B-cell lymphoma revealed by microenvironmental signatures. *Cancer Discov*. 2021;11(6):1468-1489.

48. Steidl C, Lee T, Shah SP, et al. Tumor-associated macrophages and survival in classic Hodgkin's lymphoma. *N Engl J Med*. 2010;362(10):875-885.

49. Steen CB, Liu CL, Alizadeh AA, Newman AM. Profiling cell type abundance and expression in bulk tissues with CIBERSORTx. *Methods Mol Biol*. 2020;2117:135-157.

50. Fangazio M, Ladewig E, Gomez K, et al. Genetic mechanisms of HLA-I loss and immune escape in diffuse large B cell lymphoma. *Proc Natl Acad Sci U S A*. 2021;118(22):e2104504118.

51. Gubin MM, Vesely MD. Cancer immunoediting in the era of immuno-oncology. *Clin Cancer Res*. 2022;28(18):3917-3928.

52. O'Donnell JS, Teng MWL, Smyth MJ. Cancer immunoediting and resistance to T cell-based immunotherapy. *Nat Rev Clin Oncol*. 2019;16(3):151-167.

53. Aoki T, Chong LC, Takata K, et al. Single-cell profiling reveals the importance of CXCL13/CXCR5 axis biology in lymphocyte-rich classic Hodgkin lymphoma. *Proc Natl Acad Sci U S A*. 2021;118(41):e2105822118.

54. Cohen Shvefel S, Pai JA, Cao Y, et al. Temporal genomic analysis of homogeneous tumor models reveals key regulators of immune evasion in melanoma. *Cancer Discov*. 2025;15(3):553-577.

55. Andor N, Graham TA, Jansen M, et al. Pan-cancer analysis of the extent and consequences of intratumor heterogeneity. *Nat Med*. 2016;22(1):105-113.

56. Sugawara T, Miya F, Ishikawa T, et al. Immune subtypes and neoantigen-related immune evasion in advanced colorectal cancer. *iScience*. 2022;25(2):103740.

57. McGranahan N, Furness AJ, Rosenthal R, et al. Clonal neoantigens elicit T cell immunoreactivity and sensitivity to immune checkpoint blockade. *Science*. 2016;351(6280):1463-1469.

58. Kurtz DM, Scherer F, Jin MC, et al. Circulating tumor DNA measurements as early outcome predictors in diffuse large B-cell lymphoma. *J Clin Oncol*. 2018;36(28):2845-2853.

59. Kurtz DM, Soo J, Co Ting Keh L, et al. Enhanced detection of minimal residual disease by targeted sequencing of phased variants in circulating tumor DNA. *Nat Biotechnol*. 2021;39(12):1537-1547.

60. Morin RD, Arthur SE, Hodson DJ. Molecular profiling in diffuse large B-cell lymphoma: why so many types of subtypes? *Br J Haematol*. 2022;196(4):814-829.

61. Müller MF, Ibrahim AE, Arends MJ. Molecular pathological classification of colorectal cancer. *Virchows Arch*. 2016;469(2):125-134.

62. Cuceu C, Colicchio B, Jeandidier E, et al. Independent mechanisms lead to genomic instability in Hodgkin lymphoma: microsatellite or chromosomal instability (dagger). *Cancers (Basel)*. 2018;10(7):233.

63. Weniger MA, Küppers R. Molecular biology of Hodgkin lymphoma. *Leukemia*. 2021;35(4):968-981.

64. Tiacci E, Döring C, Brune V, et al. Analyzing primary Hodgkin and Reed-Sternberg cells to capture the molecular and cellular pathogenesis of classical Hodgkin lymphoma. *Blood*. 2012;120(23):4609-4620.

65. Basso K, Dalla-Favera R. Germinal centres and B cell lymphomagenesis. *Nat Rev Immunol*. 2015;15(3):172-184.

66. Hoeller S, Zihler D, Zlobec I, et al. BOB.1, CD79a and cyclin E are the most appropriate markers to discriminate classical Hodgkin's lymphoma from primary mediastinal large B-cell lymphoma. *Histopathology*. 2010;56(2):217-228.

67. Tzankov A, Zimpfer A, Lugli A, et al. High-throughput tissue microarray analysis of G1-cyclin alterations in classical Hodgkin's lymphoma indicates overexpression of cyclin E1. *J Pathol*. 2003;199(2):201-207.

68. Rengstl B, Newrzela S, Heinrich T, et al. Incomplete cytokinesis and re-fusion of small mononucleated Hodgkin cells lead to giant multinucleated Reed-Sternberg cells. *Proc Natl Acad Sci U S A*. 2013;110(51):20729-20734.

69. Dietrich C, Trub A, Ahn A, et al. INX-315, a selective CDK2 inhibitor, induces cell cycle arrest and senescence in solid tumors. *Cancer Discov*. 2024;14(3):446-467.